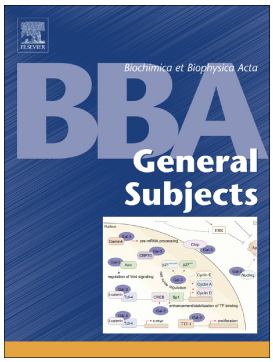

Disulfide bond formation protects Arabidopsis thaliana glutathione transferase tau 23 from oxidative damage

Maria-Armineh Tossounian, Inge Van Molle, Khadija Wahni, Silke Jacques, Kris Gevaert, Frank Van Breusegem, Didier Vertommen, David Young, Leonardo Astolfi Rosado, Joris Messens

PII: S0304-4165(17)30328-8
DOI: doi:10.1016/j.bbagen.2017.10.007
Reference: BBAGEN 28961

To appear in:

Received date: 13 June 2017
Revised date: 4 October 2017
Accepted date: 10 October 2017

Please cite this article as: Maria-Armineh Tossounian, Inge Van Molle, Khadija Wahni, Silke Jacques, Kris Gevaert, Frank Van Breusegem, Didier Vertommen, David Young, Leonardo Astolfi Rosado, Joris Messens , Disulfide bond formation protects Arabidopsis thaliana glutathione transferase tau 23 from oxidative damage. The address for the corresponding author was captured as affiliation for all authors. Please check if appropriate. Bbagen(2017), doi:10.1016/j.bbagen.2017.10.007

Disulfide bond formation protects *Arabidopsis thaliana* glutathione transferase tau 23 from oxidative damage

Maria-Armineh Tossounian,[a,b,c] Inge Van Molle,[a,b,c] Khadija Wahni,[a,b,c] Silke Jacques,[d,e,f,g,1] Kris Gevaert,[d,e] Frank Van Breusegem,[f,g] Didier Vertommen,[h] David Young, [a,b,c] Leonardo Astolfi Rosado,[a,b,c] and Joris Messens[a,b,c,2]

[a]VIB-VUB Center for Structural Biology, B-1050 Brussels, Belgium.
[b]Brussels Center for Redox Biology, B-1050 Brussels, Belgium.
[c]Structural Biology Brussels, Vrije Universiteit Brussel, B-1050 Brussels, Belgium.
[d]VIB-UGent Center for Medical Biotechnology, B-9000, Ghent, Belgium.
[e]Department of Biochemistry, Ghent University, B-9000 Ghent, Belgium,
[f]VIB-UGent Center for Plant Systems Biology, Technologiepark 927, B-9052 Ghent, Belgium. [g]Department of Plant Biotechnology and Bioinformatics, Ghent University, Technologiepark 927, B-9052 Ghent, Belgium.
[h]de Duve Institute, Université Catholique de Louvain, 1200 Brussels, Belgium

[1]Current address: Centre for Environment and Life Sciences, CSIRO Agriculture, Western Australia
[2]To whom correspondence should be addressed: Joris Messens, VIB-VUB Center for Structural Biology, Oxidative Stress Signaling lab, Vrije Universiteit Brussel (VUB), Pleinlaan 2, 1050 Brussels, Belgium, Phone: +32 2 6291992, Fax: +32 2 6291963; E-mail: joris.messens@vib-vub.be

Abbreviations: AEBSF, 4-(2-aminoethyl) benzenesulfonyl fluoride hydrochloride; AU, asymmetric unit; CDNB, 1-Chloro-2,4-dinitrobenzene; CD, circular dichroism; GSH, glutathione; GST, glutathione S transferase; GSTU23, glutathione S transferase Tau23;IPTG, isopropyl β-D-1-thiogalactopyranoside; Met-*S*-SO & Met-*R*-SO, R and S epimeric forms of methionine sulfoxide; $MetSO_2$, methionine sulfone; Msr, methionine sulfoxide reductase; ROS, reactive oxygen species

Abstract

Background: Glutathione transferases play an important role as detoxifying enzymes. In *A. thaliana*, elevated levels of reactive oxygen species (ROS), provoked during biotic and abiotic stress, influence the activity of GSTU23. The aim of this study is to determine the impact of oxidative stress on the function and structure of GSTU23.

Methods: The impact of oxidation on the function of GSTU23 was studied using a glutathione transferase biochemical assay and mass spectrometry. With kinetics, circular dichroism and thermodynamics, we compared reduced with oxidized GSTU23. X-ray crystal structures of GSTU23 visualize the impacts of oxidation on methionines and cysteines.

Results: In the presence of 100 μM H_2O_2, oxidation of the methionine side-chain to a sulfoxide is the prominent post-translational modification, which can be reduced by *C. diphtheriae* MsrA and MsrB. However, increasing the level to 200 μM H_2O_2 results in a reversible intramolecular disulfide between Cys65-Cys110, which is substrate for glutaredoxin. Under these oxidizing conditions, GSTU23 undergoes a structural change and forms a more favorable enzyme-substrate complex to overcome k_{cat} decrease.

Conclusions and significance: At lower H_2O_2 levels (100 μM), GSTU23 forms methionine sulfoxides. Specifically, oxidation of Met14, located near the catalytic Ser13, could interfere with both GSH binding and catalytic activation. At higher H_2O_2 levels (200 μM), the Cys65-Cys110 disulfide bond protects other cysteines and also methionines from overoxidation. This study shows the impact of oxidative stress on GSTU23 regulated by methionine sulfoxide reductases and glutaredoxin, and the mechanisms involved in maintaining its catalytic functionality under oxidizing conditions.

Keywords: Glutathione transferase, kinetics, X-ray structure, thermodynamics, methionine sulfoxide, disulfide bond

1. Introduction

Plant glutathione transferase (GST) enzymes play an important role during oxidative stress, secondary metabolism, and are involved in the detoxification of electrophilic substrates by glutathione (GSH) conjugation and by peroxide scavenging [1, 2]. Particularly, they have been shown to detoxify heavy metals [3] and herbicides [4]. Although plant GSTs share only around 10% amino acid identity between the different GST families, crystallographic studies revealed a high degree of structural conservation resulting in a highly similar overall protein fold [4-7]. They have a characteristic glutathione-binding site (G-site) and a hydrophobic site (H-site), where hydrophobic substrates bind.

The *A. thaliana* genome encodes for 55 GSTs, subdivided mainly based on sequence identity and the identity of the catalytic active site residue (Ser, Tyr or Cys) into several classes from which the plant-specific Tau class, which has a catalytic Ser, is the largest one with 28 members [8, 9]. In addition to their transferase activity, Tau GSTs also exhibit a glutathione dependent peroxidase activity [10-12], and they contribute to plant resistance mechanisms under biotic and abiotic stress [1, 13]. Under such stress conditions, elevated levels of reactive oxygen species (ROS) are produced, which mostly influence the protein sulfurous amino acids cysteine (Cys) [14] and methionine (Met) [15]. Upon oxidation, Cys residues react to form sulfenic (RSOH), sulfinic (RSO_2H), sulfonic acid (RSO_3H) depending on the level of oxidant and location of the residue, or inter/intra-molecular disulfide bonds are formed [16, 17]. Some of these modifications are demonstrated to be involved in protein function regulation [18], and can be recycled by the thioredoxin or the glutathione (GSH) system [19-21]. On the other hand, modifications such as sulfinic and sulfonic acids are irreversible. When sulfurs of methionines are oxidized, it leads to the formation of two epimeric forms of methionine sulfoxide (Met-*S*-SO and Met-*R*-SO), which more recently emerged as a trigger for redox regulation [22, 23]. There are two major types of stereospecific methionine sulfoxide reductases: MsrA, specifically reduces Met-*S*-SO [24], and MsrB reduces Met-*R*-SO [25]. Under highly oxidizing conditions, methionine sulfoxide can further oxidize to the irreversible form methionine sulfones ($MetSO_2$), which can interfere with protein function and can even lead to loss of protein function [15, 26]. To protect proteins from such over-oxidation, *A. thaliana* expresses up to 5 MsrA and 9 MsrB proteins, which are localized at different cellular compartments and thus can prevent methionine over-oxidation through recycling of generated methionine sulfoxides [27, 28], underlining their potential in oxidative stress regulation. An example of such a case has been shown for *A. thaliana* GST Phi2 (GSTF2) and GST Phi3 (GSTF3), where oxidation of these proteins leads to methionine sulfoxide formation, which is stereospecifically reduced back to methionine by MsrB7 and confer oxidative stress tolerance to transgenic *A. thaliana* overexpressing MsrB7 [29]. This

example for Phi class GSTs shows the crucial role of stereospecific methionine sulfoxide reductases in regulating enzyme functions.

In *A. thaliana* leaves exposed to oxidative stress, we recently mapped over 500 sites of methionine oxidation in about 400 proteins and demonstrated the negative impact of Met oxidation on the activity of recombinant glutathione transferase GSTF9 and GSTU23 [30].
Here, we present structural and functional insights into the redox modulation mechanisms used by GSTU23 under oxidative stress. We found that at lower levels of hydrogen peroxide (100 µM), MetSO is the major post-translational modification, reducing its transferase activity. The methionine sulfoxide reductases, MsrA and MsrB, restore the transferase activity. In the X-ray structure of oxidized GSTU23, we visualized MetSO formation on specific methionines, Met14 and Met47. We also showed that Met14 is sensitive to oxidation, which could negatively interfere with the binding of GSH to the G-site or the activation of the catalytic Ser13 located close to Met14. At 200 µM H_2O_2, the major post-translational modification observed is the disulfide bond formation between Cys65 and Cys110, which negatively affects the transferase activity. This disulfide protects both cysteines and methionines from over-oxidation. In addition, our study shows that oxidized GSTU23, $GSTU23_{ox200}$, forms a more favorable enzyme-substrate complex with minor conformational changes compared to the reduced enzyme. We propose a fine-tuned reaction mechanism for the regulation of GSTU23 under oxidizing conditions, where Msr enzymes and disulfide bond reducing systems work together to restore GSTU23 activities.

2. Materials and methods

2.1. Expression and purification of GSTU23

The full-length Open Reading Frame of the *Arabidopsis thaliana* GSTU23 (AT1G78320) cloned in pDEST14 Gateway™ vector (Thermo Fisher Scientific) was transformed in *E. coli* Rosetta (DE3) cells. Cells were grown in Luria Broth and induced with 0.5 mM isopropyl β-d-1-thiogalactopyranoside (IPTG) at an A_{600} of 0.7. After induction, the cells were grown overnight (O/N) at 30˚C. The harvested cells were pelleted and re-suspended in an ice-cold buffer solution composed of 50 mM Tris-HCl, pH 8, 0.1 M NaCl, 1 mM DTT, 0.1 mg/mL 4-(2-aminoethyl) benzenesulfonyl fluoride hydrochloride (AEBSF), 1 µg/mL Leupeptine, 50 µg/mL DNaseI and 20 mM $MgCl_2$. The cells were lysed using a French press (Constant System) at 20 kpsi and the cell debris was removed by centrifugation at 18,000 rpm for 45 min at 4°C, using Avanti® J-26xp centrifuge (BECKMAN COULTER®). The cell lysate was directly loaded onto a glutathione Sepharose 4B (GE Healthcare) column, which was equilibrated with 50 mM Tris-HCl, pH 8, 0.1 M NaCl and 1 mM DTT at room temperature (RT) using a AKTA™ pure system (GE Healthcare, Life Sciences). The GSTU23 was then eluted with 10 mM GSH in the same buffer. Enzyme purity was assessed on a non-reducing SDS-PAGE gel.

2.2. Cloning, expression and purification of MsrB

PCR was used to amplify the *msrB* gene from the total DNA of *Corynebacterium diphtheriae* using the FW (5'-CGCGCGGCAGCCATATGACAAATTTTAAACTGATC-3') and Rv (5'-GTGCGGCCGCAAGCTTAACTCTCTTCTGCCGGAATG -3') primers. The amplified PCR product was cloned in pET28b(+) to form Cd-*msrB*-pET28b(+). The plasmid was transformed in Rosetta (DE3) *E. coli*, and cells were grown, induced, harvested and purified as described for *C. diphtheriae* MsrA with minor modifications [31]. Cell lysate was incubated in-batch for 1 h at 4˚C with Zn^{2+}-agarose beads (WorkBeads^{TM} 40 IDA^{High}, Bio-Works), equilibrated with 20 mM Tris pH 7.5, 0.5 M NaCl, 2 mM imidazole and 1 mM DTT. The beads were packed in a column and MsrB was eluted with 20 mM Tris pH 7.5, 0.5 M NaCl, 1 M imidazole and 1 mM DTT on an AKTA^{TM} pure system (GE Healthcare, Life Sciences). With size exclusion chromatography impurities were removed from the sample. The purity of the MrsB containing fraction was evaluated on a non-reducing SDS-PAGE gel.

2.3. GSTU23 oxidation

Purified GSTU23 was reduced with 10 mM DTT for 30 min at room temperature. Excess of GSH and DTT were removed on a Superdex 75 HR 10/30 size exclusion chromatography (SEC) column equilibrated in PBS buffer composed of 140 mM NaCl, 2.7 mM KCl, 1.76 mM KH_2PO_4 and 10 mM Na_2PO_4, pH 7.5. From the collected samples under the elution peak, 30 µM of GSTU23 was incubated with 100 or 200 µM hydrogen peroxide (H_2O_2) for 1 h at 25˚C to form $GSTU23_{ox100}$ and $GSTU23_{ox200}$, respectively. Excess H_2O_2 was removed by Micro Bio-Spin® Chromatography Columns (BIO-RAD), in PBS.

2.4. Glutathione transferase activity assay

The reaction was started by adding 2.5 mM 1-chloro-2, 4 dinitrobenzene (CDNB) to the reaction mixture composed of 5 mM GSH and 0.4 µM GSTU23 (reduced or oxidized form) in 250 mM MOPS, pH 6.5, 150 mM NaCl. The order of the components added was buffer, GSH, GSTU23 and finally, CDNB. The A_{340} ($\varepsilon = 9.6 \times 10^3\ M^{-1}\ cm^{-1}$) was monitored for 100 s at 25˚C in a Nunc™ MicroWell™ 96-well Microplate (Thermo Scientific) using a SpectraMax340PC spectrophotometer (Molecular Devices). The increase in A_{340} was measured in function of time, as the conjugation of GSH onto CDNB forms a product that absorbs at 340 nm [32]. To measure the influence of Msr on the activity of $GSTU23_{ox}$, a 1:10 molar ratio of $GSTU23_{ox}$ (4 µM) was incubated with *C. diphtheriae* MsrA [31] or MsrB (40 µM) for 30 min at 25ºC using PBS as a reaction buffer. Prior to the incubation, MsrA and MsrB were reduced with 20 mM DTT and excess of DTT was removed on Micro Bio-Spin® Chromatography Columns (BIO-RAD) equilibrated with PBS buffer. To measure the influence of DTT on the $GSTU23_{ox}$ activity, the latter was incubated with 2 mM DTT at 25˚C

for 40 min and the activity was measured. The control sample, with no enzyme, was treated similarly, where DTT showed no influence on the assay components. Similar conditions were used for the incubation of $GSTU23_{ox200}$ (4 µM) with reduced *Pt*-GrxC1 (gift from Jean-Pierre Jacquot) or Cg-Trx (40 µM) [31]. Important to note is that the influence of MsrA, MsrB, DTT, GrxC1 and Trx on the assay components was tested prior to the start of these assays, where increase in A_{340} was not observed.

2.5. Gel shift assay

To determine whether GSTU23 forms an inter- or intra-molecular disulfide bond in its oxidized form, GSTU23 was reduced as described in section 2.3 and 30 µM of GSTU23 was oxidized with 100 µM or 200 µM H_2O_2 for 1 h at 25˚C to form $GSTU23_{ox100}$ and $GSTU23_{ox200}$. Excess H_2O_2 was removed on Micro Bio-Spin® Chromatography Columns (BIO-RAD) in PBS buffer. Reduced GSTU23 was treated similarly. Following oxidation, the oxidized samples were incubated with 2 mM DTT at 25ºC for 40 min. The samples were then mixed with the SDS-loading dye, boiled for 10 min and loaded on a non-reducing SDS-PAGE gel. Protein bands were visualized with InstantBlue™ (Sigma).

2.6. Kinetics study of $GSTU23_{red}$ and $GSTU23_{ox200}$

The enzyme activity was monitored at 340 nm by following CDNB-GSH complex formation in function of time. The reaction was performed at 25˚C in a 500 µl final volume in quartz cuvettes (ThermoFisher Scientific), containing 100 nM $GSTU23_{red}$ or $GSTU23_{ox200}$ and 5 mM GSH directly mixed in a 250 mM MOPS, pH 6.5, 150 mM NaCl buffer solution, where the reaction started following the addition of increasing concentrations of CDNB (0.025 – 2.5 mM). The increase in absorbance was monitored with a Bio UV-visible spectrophotometer (Varian Cary 100) equipped with a temperature-controlled cuvette holder. Steady-state rates for each CDNB concentration in the presence of a saturating concentration of GSH were plotted and fitted with the Michaelis-Menten equation (1) to obtain the kinetic parameters k_{cat} and K_m. Two independent replicates of k were measured for each substrate concentration.

$$v = \frac{V_{max}[S]}{K_M + [S]} \quad (1)$$

2.7. Thermodynamic study of $GSTU23_{red}$ and $GSTU23_{ox200}$

The initial velocity variation in function of temperature was measured. The reactions were carried out at 17°C, 20°C, 25°C, 30°C and 37°C in quartz cuvettes using a UV-visible spectrophotometer and were monitored for 80 s in the presence of 100 nM GSTU23 (reduced or oxidized) in a 250 mM MOPS, pH 6.5, 150 mM NaCl buffer solution. Two independent replicates were measured. Subsequently, the thermodynamic parameters were obtained fitting the data with an Arrhenius plot (2) and the Eyring plot (3). For equation (2), E_a is the reaction

activation energy, R is the gas constant (8.314 $J.mol^{-1}K^{-1}$) and A is the product of the collision frequency (Z). For equation (3), k_B is the Boltzmann constant ($1.3805x10^{-23}$ $J.K^{-1}$), h is the Planck's constant ($6.6256x10^{-34}$ J.s), $\Delta H^{\#}$ and $\Delta S^{\#}$ are the enthalpy and entropy variation of activation.

$$lnk = -\frac{E_a}{R}\frac{1}{T} + lnA \quad (2)$$

$$ln\left(\frac{k}{T}\right) = -\frac{\Delta H^{\#}}{R}\frac{1}{T} + \frac{\Delta S^{\#}}{R} + \ln\left(\frac{k_b}{h}\right) \quad (3)$$

The Gibbs free energy of activation ($\Delta G^{\#}$) was calculated using the relationship

$$\Delta G^{\#} = \Delta H^{\#} - T\Delta S^{\#} \quad (4)$$

The Gibbs free energy of the E:S complex formation was calculated using the relationship described below, where K_{eq} corresponds to $1/K_m$.

$$\Delta G° = -RT.\ln K_{eq} \quad (5)$$

2.8. Crystallization, X-ray data collection and structure refinement of GSTU23

Prior to crystallization, GSTU23 was reduced with 10 mM DTT at RT and further purified by Superdex 75 HR 10/30 SEC into a 50 mM Tris-HCl, pH 8, 100 mM NaCl and 1 mM DTT buffer solution using an AKTA™ pure system (GE Healthcare, Life Sciences) at RT. The protein was then concentrated to 20 mg/mL using a Vivaspin 10 kDa cut-off concentrator.

Reduced GSTU23 was crystallized using the hanging drop vapor diffusion method in 0.16 M $MgCl_2$, 0.08 M Tris-HCl pH 8.5, 24% PEG 4000 and 20% glycerol with a 1:1 ratio of protein to precipitant solution at 10ºC. Crystals of GSTU23 were flash-frozen in liquid nitrogen in the crystallization condition. To obtain a GSH-bound structure, crystals of GSTU23 were soaked for 5 h in 1 mM GSH, dissolved in the same solution as mentioned above. To determine the effect of oxidation, GSTU23 crystals were soaked overnight in the crystallization condition containing 0.5 M H_2O_2 plus 1 mM NaOCl.

X-ray data for GSTU23 crystals were collected at 100 K at the Diamond Light Source (DLS) synchrotron facility and on a Rigaku MicroMax-007 in house X-ray source. X-ray data were processed using XDS [33]. The GSTU23 structure was solved using the wheat GSTU4-4 structure (PDB ID: 2VO4) as a template. The GSTU23 model was subsequently build manually in Coot [34], and iteratively refined using phenix.refine [35] from the Phenix suite. X-ray data collection, processing and refinement parameters are summarized in Table 3. All structural figures were prepared using PyMOL [36].

2.9. Secondary structural changes studied by circular dichroism

GSTU23 was reduced with 10 mM DTT at room temperature for 30 min. Following reduction, excess of DTT was removed using Micro Bio-Spin® Chromatography Columns (BIO-RAD) equilibrated in PBS buffer. The samples (30 µM) were then oxidized with 100, 200 and 500 µM H_2O_2 in PBS for 1 h at 25°C to have $GSTU23_{ox100}$, $GSTU23_{ox200}$ and $GSTU23_{ox500}$, and the excess of oxidant was removed using Micro Bio-Spin® Chromatography Columns (BIO-RAD) equilibrated with 50 mM ammonium bicarbonate pH 7.4. Following sample preparation, 4 µM of sample was analyzed on a Jasco J-810 spectropolarimeter at 25°C in a quartz cuvette with a 1-mm path length. Far-UV CD spectra were measured and the results were analyzed in GraphPad Prism7 to compare the overall secondary structures of reduced and oxidized GSTU23. The data was analyzed using exponential decay equation.

$$Y = (Y0 - Y_{max}).e^{(-K.X)} + Y_{max} \quad (6)$$

2.10. Mass spectrometric analysis of Met oxidation and disulfide bond formation

The reduced ($GSTU23_{red}$) and oxidized ($GSTU23_{ox100}$ and $GSTU23_{ox200}$) samples were prepared as described in 2.4. Briefly, following oxidation, the samples were passed through the Micro Bio-Spin® Chromatography Columns (BIO-RAD) to remove excess of H_2O_2. The samples were then incubated for 10 min in the dark with 4 mM N-ethylmaleimide (NEM), an alkylating agent, which blocks free Cys thiols. Following blocking, mass spectrometry was used to analyze the samples.

For the identification of oxidized Cys and Met residues, the proteins were desalted and concentrated by methanol/chloroform precipitation prior to an overnight endo-GluC or chymotrypsin digest in 50 mM NH_4HCO_3, pH 8.0 at 30°C. The reaction was stopped by the addition of trifluoroacetic acid to a final concentration of 0.1%. The peptides were analyzed by LC-MS/MS in a microelectrospray ionization ion trap mass spectrometer (Orbitrap LTQ XL, Thermo Scientific, San José, CA) as described [37]. The mass spectrometer was operated in data-dependent-mode and switched automatically between MS and MS/MS. Zoom Scan for charge state determination (mass range 300-2000 m/z) and MS/MS with collision energy of 30% was set for sequence information. This process was repeated for the five most abundant ions. Dynamic exclusion was enabled to allow analysis of co-eluting peptides, the exclusion size list was set to 250 and the exclusion duration to 60 seconds. For peptide identification, peak lists were generated using the application spectrum selector in the Proteome Discoverer 1.4 package. The resulting peak lists were searched using Sequest HT against a homemade protein database containing the GSTU23 sequence from *Arabidopsis thaliana* (UniProt Q9M9F1). The following parameters were used: GluC with cleavage only

after glutamic acid; chymotrypsin with cleavage only after tryptophan, tyrosine, phenylalanine and leucine; the number of allowed missed cleavage sites was set to 1 for GluC and to 3 for chymotrypsin; the mass tolerance for precursor and fragment ions was 0.5 Da, and the considered dynamic modifications were +16.00 Da or +32.00 Da for oxidized methionine (sulfoxide or sulfone), +32.00 Da or + 48.00 Da for oxidized cysteine (sulfinic or sulfonic) and + 125.00 Da for NEM. Peptide matches were filtered using the q-value and Posterior Error Probability calculated by the Percolator algorithm ensuring an estimated false positive rate below 5% and manually validated. The mixed disulfide were identified by the use of the DBond software [38]. Briefly to identify disulfide-linked peptides from an MS/MS spectrum, candidate peptide pairs are obtained by database search. For each peptide pair, both component peptides should include Cys, and the sum of their molecular weights minus 2 Da (mass of -2H) should be matched to the mass of the precursor ion. Then, each peptide pair obtained as such generates fragment ions according to the linked structure, and they are compared with fragmentation information from its MS/MS spectrum. The specific disulfide bond site is then determined by scoring and manually validated.

2.11. $GSTU23_{ox}$ recycling by glutaredoxin in the GSH/glutathione reductase/NADPH pathway

The $GSTU23_{ox200}$ was reduced and oxidized at 25°C as described in section 2.3. Following oxidation, Micro Bio-Spin® Chromatography Column (BIO-RAD) equilibrated in PBS was used to remove excess of H_2O_2. The enzymatic assay performed as described in Van Laer *et al*. [39] and adapted to include $GSTU23_{ox200}$. Briefly, the reaction mixture composed of 0.5 mM NADPH, 0.5 µM glutathione reductase (GR) (Baker's yeast, Sigma), 2 µM *Pt*-GrxC1 and 0.5 mM GSH in PBS buffer was incubated for 10 min at 25°C in a final reaction volume of 150 µL. Following the incubation, $GSTU23_{ox200}$ (16 µM) was added to start the reaction and NADPH consumption was monitored at A_{340} in a Nunc™ MicroWell™ 96-well Microplate (Thermo Scientific) using a SpectraMax340PC spectrophotometer (Molecular Devices) at 25°C. As control the reaction was performed in the absence of Grx and in the presence of $GSTU23_{red}$. To test whether the reaction is performed under rate-limiting conditions for $GSTU23_{ox}$ reduction, two concentrations of $GSTU23_{ox200}$ were tested, 8 and 16 µM, where doubling of k (s^{-1}) was observed upon doubling of $GSTU23_{ox200}$ concentration.

2.12. $GSTU23_{ox200}$ recycling by the thioredoxin/thioredoxin reductase/NADPH pathway

The $GSTU23_{ox200}$ was reduced and oxidized at 25°C as described in section 2.3. Following oxidation, Micro Bio-Spin® Chromatography Column (BIO-RAD) equilibrated in PBS was used to remove excess of H_2O_2. The enzymatic assay performed as described by Tossounian *et al*. [31] and adapted to include $GSTU23_{ox200}$. Briefly, the reaction mixture

composed of 0.5 mM NADPH, 3 µM *C. glutamicum* thioredoxin reductase (TrxR), 1.5 µM *C. glutamicum* thioredoxin [40] in PBS buffer was incubated for 10 min at 25°C with a final reaction volume of 150 µL. The reaction started following the addition of 16 µM $GSTU23_{ox200}$ and NADPH consumption was monitored at A_{340} in a Nunc™ MicroWell™ 96-well Microplate (Thermo Scientific) using a SpectraMax340PC spectrophotometer (Molecular Devices) at 25°C. As control the reaction was performed in the absence of Trx.

2.13. Site-directed mutagenesis, expression and purification of GSTU23 C65S and C110S mutants

To obtain the GSTU23 C65S and C110S mutants, site-directed mutagenesis was performed on the *gst*U23 - pDEST14 vector using the QuikChange™ site-directed mutagenesis protocol (Stratagene). The forward primers 5'- GGT AAA CCG ATC TCC GAA TCG ATA ATC C-3' and 5'- G ACA TAC GTG CCA TCC AAG GCA TTA TGG -3' and reverse primers 5'- G GAT TAT CGA TTC GGA GAT CGG TTT ACC-3' and 3'- CCA TAA TGC CTT GGA TGG CAC GTA TGT C -5' were used to construct C65S and C110S GSTU23 mutants respectively. The expression and purification of the two mutants is the same as in section 2.1, with the exception of using BL21 (DE3) instead of Rosetta expression cells.

2.14. GSTU23 FOX assay

The glutathione peroxidase activity of GSTU23 was monitored using the FOX assay [41]. The sample containing 50 µM GSTU23 (reduced or oxidized forms), 1 mM GSH and 150 µM H_2O_2 in 100 mM potassium phosphate buffer at pH 6.4 was incubated at RT. At three time points (1, 2.5, 5, 10 and 15 min), 10 µL of sample was mixed with 490 µL of the FOX assay mixture composed of xylenol orange (100 µM), sorbitol (100 mM), ammonium ferrous sulphate (250 µM) and H_2SO_4 (25 mM), and further incubated in the dark at RT. After 30 min, the absorption at 560 nm was measured using a SpectraMax340PC spectrophotometer (Molecular Devices) at 25°C. Three independent measurements were performed and the data were fitted exponentially using GraphPad prism7.

2.15. Accession codes

The structures of $GTSU23_{red}$ (PDB ID: 5FQY), $GSTU23_{GSH}$ (PDB ID: 5FR4), $GSTU23_{ox}$ (PDB ID: 5O84) have been deposited in the Protein Data Bank.

3. Results

3.1. Oxidation decreases the transferase activity of GSTU23

A proteomic study of *A. thaliana* leaves exposed to oxidative stress has uncovered 500 sites of methionine sulfoxide on about 400 proteins, with an effect on the transferase activity of GST Phi 9 (GSTF9) and GST Tau 23 (GSTU23) [30]. In this follow-up study, we focused on the redox regulation mechanisms and the effect of the oxidation on the structure and function of GSTU23. Therefore, GSTU23 was recombinantly overexpressed, purified to homogeneity and oxidized with 100 µM ($GSTU23_{ox100}$) or 200 µM ($GSTU23_{ox200}$) H_2O_2. Following oxidation, the oxidant was removed and the effect of oxidation on GSTU23 transferase activity was evaluated by monitoring the conjugation of GSH to 1-chloro-2, 4-dinitrobenzene (CDNB) at 340 nm in function of time [32], and this at different H_2O_2 concentrations (Fig. 1). By measuring the activity of $GSTU23_{ox100}$, a significant ($p \leq 0.005$) decrease of 33% of the initial velocity compared to the activity of reduced GSTU23 was observed (Fig. 1A). For $GSTU23_{ox200}$, a significant ($p \leq 0.005$) decrease of 59% was observed. This shows that at increasing concentrations of H_2O_2, the transferase activity is influenced differently, which might be due to distinct oxidative modifications on GSTU23.

3.2. The oxidative modifications are reversible and H_2O_2 concentration dependent

To validate the nature of the drop of GSTU23 transferase activity, its reversibility with stereospecific methionine sulfoxide reductases A and B (MsrA or MsrB) was tested [31]. A 100 µM H_2O_2 treated GSTU23 sample ($GSTU23_{ox100}$) was incubated for 30 min with 10-molar excess of reduced Msr enzymes and the transferase initial velocities were measured (Fig. 1A). We found a recovery up to ~90% of the initial transferase activity, which indicates that GSTU23 loss of activity is primarily due to the formation of Met-*R*,*S*-SO. However, after doubling the H_2O_2 concentration to 200 µM ($GSTU23_{ox200}$), neither MsrA nor MsrB could fully recover the loss of activity (Fig. 1B), indicating that the nature of these oxidative modifications is distinct from methionine sulfoxidation. Therefore, $GSTU23_{ox100}$ and $GSTU23_{ox200}$ were incubated for 40 min with a 500-molar excess of DTT (Fig. 1). This resulted in a marginal recovery of the initial transferase activity of $GSTU23_{ox100}$ and a ~90% recovery of the initial transferase activity of $GSTU23_{ox200}$ (Fig. 1A and B). All in all, these results show that the oxidation of GSTU23 is reversible, and its nature depends on the H_2O_2 concentration.

3.3. Oxidized GSTU23 is recycled by a Grx dithiol mechanism

To explore whether oxidized GSTU23 can be reduced by a physiological reductive recycling pathway, $GSTU23_{ox200}$ was tested as substrate for both reduced glutaredoxin (Grx) and thioredoxin (Trx). $GSTU23_{ox200}$ was incubated for 40 min with 10-molar excess of reduced Grx or Trx and the transferase activity was recorded. The results showed that only Grx could recover the initial transferase activity of $GSTU23_{ox200}$ up to 97% (Fig. 2A). These

results were also confirmed by using $GSTU23_{ox200}$ as substrate for the GSH/GR/NADPH and Trx/TrxR/NADPH pathway, where coupling to the GSH/GR/NADPH pathway showed a rate constant (*k*) of 0.01 s^{-1}, while coupling to the Trx/TrxR/NADPH pathway showed no NADPH consumption (Fig. 2B).

3.4. GSTU23 oxidation results in methionine sulfoxide and cysteine disulfide formation

To get further insight into the nature of the H_2O_2-induced oxidative modifications at the sulfur sites, we analyzed 100 µM and 200 µM oxidized GSTU23 following oxidant removal and free-thiol blockage with NEM, by mass spectrometry. In $GSTU23_{ox100}$, we observed sulfoxidation of both Met47 and Met183, while the peptides carrying the other Met residues were not detected (Fig. 3 and Table 1). In addition, the presence of a Cys65-Cys110 disulfide was observed (Table 1), but since the Msr-enzymes were able to recover the $GSTU23_{ox100}$ transferase activity, we reasoned that at 100 µM H_2O_2 the major form of modification is sulfoxidation. On the other hand, MS analysis of $GSTU23_{ox200}$ showed the presence of disulfide bonds between Cys65-Cys110 (Fig. 3B), Cys65-Cys189 and Cys110-Cys110 (Table 1).

To determine whether the disulfide bonds identified by mass spectrometry are inter- or intra-molecular disulfide bonds, $GSTU23_{red}$, $GSTU23_{ox100}$ and $GSTU23_{ox200}$ were analyzed on non-reducing SDS gel in reducing (+DTT) and non-reducing (-DTT) conditions (Fig. S1). Throughout all the samples, no higher molecular weight bands were observed, indicating an absence of inter-molecular disulfide formation. Hence, the mass spectrometry analysis, which showed the presence of an inter-molecular Cys110-Cys110 disulfide bond, must be considered as a minor form within the population or a MS artifact.

To further understand the impact of the oxidation on the cysteines, two Cys to Ser mutants (C65S and C110S) were constructed and the glutathione transferase activities were compared under oxidative conditions (Fig. 4-A, B and C). Whereas oxidation of WT GSTU23 with 100 and 200 µM H_2O_2 decreases the transferase activity to 67% and 41% (Fig. 4-A), respectively, oxidation of the C65S variant has no effect on its transferase activity (Fig. 4-B). The GSTU23 C110S variant, retained its sensitivity to oxidative inactivation, displaying a decrease in transferase activity to 91% and 67% upon treatment with 100 and 200 µM H_2O_2, respectively, indicating the sensitivity of Cys65 to H_2O_2 oxidation with an impact on the transferase activity (Fig. 4C).

Altogether, the major oxidation of $GSTU23_{ox200}$ is due to intra-molecular disulfide bond formation, which confirms activity recovery with DTT and Grx (Fig. 1B and 2). On the other hand, Met oxidation was not detected in the $GSTU23_{ox200}$ sample, indicating that disulfide bond formation protects against Met oxidation.

3.5. Oxidation affects GSTU23 kinetics

As the oxidation of GSTU23 with 200 μM H_2O_2 caused a significant decrease of transferase activity to 41%, we determined the steady-state kinetic parameters of $GSTU23_{red}$ and $GSTU23_{ox200}$. Initial velocities were plotted against increasing concentrations of CDNB in the presence of saturating concentration of GSH (5 mM) and data were fitted with the Michaelis-Menten equation (Fig. 5). We found that the k_{cat} decreases 5.1-fold upon oxidation with 200 μM H_2O_2, from 3.6 ± 0.1 s^{-1} to 0.7 ± 0.02 s^{-1} for $GSTU23_{red}$ and $GSTU23_{ox200}$, respectively (Fig. 5). On the other hand, also the K_m decreases 6.6-fold upon oxidation, from 530 ± 40 μM to 80 ± 10 μM, which makes that the final effect on k_{cat}/K_m is almost completely cancelled out with values of 6.79 x10^3 $M^{-1}s^{-1}$ and 8.75 x10^3 $M^{-1}s^{-1}$ for $GSTU23_{red}$ and $GSTU23_{ox200}$, respectively. This indicates that under oxidizing conditions, GSTU23 copes by a k_{cat}/K_m compensatory mechanism.

3.6. $GSTU23_{ox200}$ forms a more favourable enzyme:substrate complex to overcome k_{cat} decrease

To further understand how the formation of disulfide bonds affect the catalytic efficiency of GSTU23, the transition state thermodynamic parameters ($\Delta H^{\#}$, $\Delta S^{\#}$ and $\Delta G^{\#}$) and the energy of activation (E_a) were determined for $GSTU23_{red}$ and $GSTU23_{ox200}$ (Table 2, Fig. 6 and Fig. S2). After measuring the temperature dependency of the rate constant k_{cat} (s^{-1}), the E_a was estimated by the slope of the Arrhenius plot ($-E_a/R$) (Fig. S2). The Eyring plot was utilized to estimate the transition state thermodynamic parameters where the slope is defined as $-\Delta H^{\#}/R$ and the intercept as $\Delta S^{\#}/R + \ln k_b/h$. Comparison of E_a and $\Delta H^{\#}$ of $GSTU23_{red}$ and $GSTU23_{ox200}$ demonstrates that the $E:S_{red}$ state requires 4 kcal.mol^{-1} less to reach the transition state conformation compared to its oxidized counterpart. On the other hand, $E:S_{ox200}$ activation is 3.3 kcal.mol^{-1} more favourable than $E:S_{red}$ activation. These values lead to an enthalpy-entropy compensatory system, where the $\Delta G^{\#}$ values revealed a $\Delta\Delta G^{\#}$ of 0.7 kcal.mol^{-1} (Table 2). Since activation parameters are the difference in energy from the activated $E:S^{\#}$ complex and the E:S ground state, we sought to investigate the energy profile of the E:S complex formation. It has been demonstrated that GST enzymes catalysing the conjugation of GSH and CDNB are under a rapid-equilibrium random mechanism [42-46]. Assuming that GSTU23 is also under a rapid-equilibrium mechanism, K_m can be considered as K_D and a $\Delta G°$ for the E:S complex formation can be calculated [47]. The conversion of K_m values in $\Delta G°$ utilizing equation 5 revealed a more favourable complex formation for $E:S_{ox200}$ (-5.5 ± 0.7 kcal.mol^{-1}) in contrast with the $E:S_{red}$ form (-4.4 ± 0.3 kcal.mol^{-1}). These results suggest that $GSTU23_{ox200}$ has higher affinity for CDNB to overcome the decrease in activity occasioned

by disulfide bond formation in a similar mechanism observed for mesophilic and psychrophilic (cold adapted) enzymes (Fig. 6).

3.7. Overall GSTU23 X-ray crystal structure

The crystal structures of reduced, GSH-bound and oxidized GSTU23 were solved to resolutions of 1.59 Å, 1.95 Å and 1.88 Å respectively. All structures exhibited a structural topology common to the GST superfamily, consisting of an N-terminal thioredoxin-like domain and C-terminal helical bundle domain (Fig 7A). All three structures of GSTU23 were obtained in the *C*2 space group, and crystallized as a homodimer with 2 subunits of GST in the asymmetric unit for the reduced and GSH-bound structures, and 1 subunit of GSTU23 in the case of the oxidized structure, related to its partner subunit by crystallographic symmetry. We highlighted the respective location of Cys and Met residues in the structure of GSTU23 (Fig. S3). Cys65 and Cys110 are located close to the G and H-sites, respectively, while Cys189 is located at the reverse face of GSTU23. The location of Cys189 would make the disulfide formation between Cys65-Cys189 highly unlikely, as the enzyme would require a huge structural change. Within the active site, Met14 and Met17 are near the catalytic Ser13, and Met47 close to Cys65 (Fig. S3). Oxidation of the sulfurs of these Cys and Met residues could influence the catalytic activity of GSTU23.

3.8. GSH interacts with catalytic Ser13 in the G-site

The structure of $GSTU23_{GSH}$ reveals the presence of GSH within the G-site and a glycerol molecule (GOL) in the H-site, (Fig. 7A). Figures 8B and C show the stabilization interactions, which hold GSH in the G-site, where the γ-Glu moiety of GSH makes hydrogen bonds with Glu66 and Ser67, and the glycyl moiety is H-bonded to Lys40 and Lys53. The backbone of the Cys group is H-bonded to the backbone of Ile54. In addition, several H-bonds with water molecules in the active site are formed, where water 1 (W1, Fig 7D) is stabilized by the side chains of Ser67, Ile68 and the main chain of Asp103, and water 2 (W2) is stabilized by Glu66 and Pro55, respectively (Fig. 7B and C). In the substrate binding H-site, a glycerol molecule was found H-bonded with the GSH molecule of the G-site and with Tyr167. In addition to the different stabilization interactions of GSH within the G-site, the GSH thiol is oriented towards the catalytic Ser13 hydroxyl group, which is located at a distance of 2.9 Å. Upon GSH binding within the G-site, Tyr107 shows a slight shift away from the G-site, and is stabilized by Lys53, instead of the water molecule (W4) (Fig. 7D). While the catalytic Ser13 makes stabilization interactions with a water molecule (W3), upon GSH binding, this water molecule is replaced by the thiol group of GSH-Cys. Within the GSH-bound GSTU23 H-site, the glycerol molecule replaces the water molecules, and

interacts with Tyr167 via a water molecule and also with the GSH molecule within the G-site.

3.9. Methionine sulfoxide visualized in GSTU23 crystals

To elucidate structural modifications occuring upon oxidation, GSTU23 crystals were soaked overnight with 500 mM H_2O_2 and 1 mM NaOCl. Following crystallographic refinement to a resolution of 1.88 Å, oxidative modifications on the sulfurs of methionines 14 and 47, and cysteines 65 and 110 were visualized (Fig. 8, Fig. S3). Met14 was found to be over-oxidized to methionine sulfone, with oxygen occupancies refined to 100% and 53%, and Met47 was found oxidized to methionine *S*-sulfoxide, with an oxygen occupancy of 78% (Fig. 8A and B). Cys65 was observed to form a sulfinic acid, with full occupancy of its additional oxygens (Fig. 8C), which confirms its sensitivity to oxidation (Fig. 4C). A blob of ambiguous electron density was found close to the sulfinylated Cys65. A molecule of ethane-1,2-diol was tentatively placed into this density in two conformations; though it should be noted that this ligand placement is done with low confidence.

The largest oxidation-induced structural change was found to occur at Cys110, where partial unfolding of the α-helix containing Cys110 results in a reorientation of Cys110 into the central cleft of the H/G-site (Fig. 9, Fig. S3). The reorientation of Cys110 into the H-site results in the displacement of 3 water molecules by the Cys-persulfenate which are otherwise present in the crystal structure of the reduced form. Two more water molecules of the reduced structure proximal to Cys110 and Met14 are displaced by the binding of acetate in the oxidized structure. In this oxidized structure of GSTU23, Cys110 occupies two rotameric conformations, one in which the cysteine is reduced and directed towards the oxidized Met14, which forms a hydrogen bond with a nearby acetate molecule, and in the other conformation, Cys110 is oxidized, though the exact oxidative modification is ambiguous. Additional density in the omit map appears to suggest the partial formation of a persulfenate ($-SOO^-$) at the cysteine thiol (Fig. 10). Attempted placement of a partial-occupancy H_2O_2 molecule at this additional density instead results in an unfeasibly short non-bonded interaction distance between the peroxide oxygen and thiol of Cys110 of 2.17 Å, and attempts to model a water molecule in place of H_2O_2 also proved unsatisfactory. Cysteine persulfenates have been observed previously in the crystal structures of cysteine dioxygenase as reaction intermediates in the Fe-catalyzed dioxygenation of cysteine [48, 49]. However, as a cysteine persulfenate is not a reaction intermediate in the peroxide-mediated oxidation of thiols, its presence cannot be chemically justified in this crystal structure. A possible reaction route for the generation of a persulfenate modification would by via radiation-induced formation of a thiyl radical and subsequent reaction with molecular oxygen [50]. However, this would regardless present an artefactual modification, unrepresentative of a physiologically-relevant oxidation event.

Therefore, in the deposited atomic coordinates, Cys110 is modelled as a partial-occupancy sulfenic acid. The spurious additional electron density at the cysteine sulfenate is regrettably left unmodeled.

In the reduced structure of GSTU23, Cys110 and the neighboring residues, Pro109 and Lys111, have elevated temperature factors relative to the average value for the structure. This indicates that, even under non-oxidative conditions, Cys110 and its surrounding residues exhibit some extent of conformational flexibility, and possibly alternate between the respective conformations observed in the reduced and oxidized structures. It can be postulated that oxidation of the more solvent-exposed H-site-directed Cys110 may prevent the return of Cys110 to the native conformation observed in the reduced structure. Additionally, oxidation of Met14 to a sulfoxide or sulfone also appears likely to present some steric hindrance to the motion of Cys110, and may also contribute to the locking of Cys110 in its outward, H-site-orientated conformation.

3.10. Change in overall secondary structure observed upon GSTU23 oxidation

Within the oxidized crystal structure of GSTU23, cysteine oxidation was observed, but not disulfide bond formation. The disulfide bond Cys65-Cys110 of $GSTU23_{ox200}$ would require significant conformational changes to form, thereby introducing conformational heterogeneity unsuited for crystallization attempts. To gain insights into possible structural changes upon oxidation of GSTU23, circular dichroism was used (Fig. 11). Using the far-UV region (190-260 nm), we monitored the changes in the secondary structural upon GSTU23 oxidation. To determine whether GSTU23 undergoes structural changes, we monitored the overall secondary structural changes with increasing H_2O_2 concentrations (100 µM to 500 µM) (Fig. 11A). In particular, we observed a decrease in the molar ellipticity at 208 nm upon increasing H_2O_2 concentration (Fig. 11A and 9B). At this wavelength, proteins that contain only ß-sheets have a molar ellipticity value of zero, α-helical proteins have negative molar ellipticity values and disordered proteins have molar ellipticity value close to zero. Upon oxidation of GSTU23 with a higher level of H_2O_2, a decrease in the molar ellipticity at 208 nm is observed going from 100% at 0 µM H_2O_2 to 85.6% at 500 µM H_2O_2, which indicates an increase in the overall α-helical content within the oxidized GSTU23 structure (Fig. 11B). The midpoint of the secondary structure transition is at a H_2O_2 concentration of 118 µM.

4. Discussion

Plant glutathione transferases (GSTs) play an important role in cellular protection under different biotic and abiotic stress conditions [1, 2]. The Tau (U) family of GST enzymes is unique to Plantae and is considered the largest family among the different plant

GST families. Studies performed on GSTU family members show their active role in protecting cellular damage through their GSH-transferase activity and also play a secondary role as GSH-peroxidases [51]. Due to their important role during oxidative stress and detoxification, unraveling how they are redox regulated and keep on functioning under different oxidizing conditions should provide valuable information on how plants cope with biotic and abiotic stresses using different regulatory mechanisms and anti-oxidant enzymes [52].

In a previous study, we identified the methionine sulfoxome of *A. thaliana* leaves exposed to oxidative stress [30]. Among the different sulfoxidated proteins, we identified two members of the GST families Tau and Phi; GSTU23 and GSTF9, respectively. In addition, we showed that methionine sulfoxide formation on GSTU23 results in a decrease in its transferase activity [30]. Here, we probe deeper into the influence of oxidative stress on GSTU23 function, structure, and redox regulation. To study the impact of oxidation on GSTU23 transferase activity, two different hydrogen peroxide concentrations were used. Exposure of GSTU23 to 100 µM H_2O_2 induces methionine sulfoxide formation, constituting the major redox modification of $GSTU23_{ox100}$ (Fig. 1A). The decrease in enzymatic activity caused by 100 µM H_2O_2 oxidation of GSTU23 can be recovered by the action of methionine sulfoxide reductase A and B (MsrA and MsrB), which stereospecifically reduce Met-*S*-SO and Met-*R*-SO (Fig. 1A). Although the rate of Met oxidation (~10^{-3} $M^{-1}s^{-1}$) is much slower than the rate of Cys oxidation (~20 $M^{-1}s^{-1}$) [26, 53], at 100 µM H_2O_2, the major population of sulfur oxidation is methionine sulfur oxidation. Since GSTU23 has 5 Met and 3 Cys residues (Fig. S3), one would expect the Cys residues to be oxidized faster than the Met residues. Our observation on Met oxidation preceding Cys oxidation could be due to the amino acid environment of these residues, which could render Met more prone to oxidation. In a previous study in which the methionine sulfoxome of *A. thaliana* was explored [30], Met residues susceptible to oxidation were found to be neighbored by hydrophobic amino acids (Val, Leu, Ile and Met). Taking a look at the amino acid sequence of GSTU23 (Fig. S3-A), hydrophobic amino acids are seen surrounding Met residues, where Met14 and Met17 have Ala, Tyr and Met in nearby neighboring sequence ($ASM^{14}YGM^{17}$), Met47 has three Leu residues ($LLLQM^{47}$) and Met183 has Ala and Leu ($LM^{183}A$) (Fig. S3-A).

Regulation of glutathione transferases by Msr enzymes is also observed for *A. thaliana* GSTs Phi 2 and 3 (GSTF2 and GSTF3), where oxidation with 500 µM hypochlorous acid (HOCl), an oxidant which causes methionine oxidation, leads to a drop in the transferase activity of both GSTF2 and GSTF3. From the crystal structure of GSTF2, it can be seen that the methionines reside on an α-helix buried within the dimer interface, and therefore seem relatively inaccessible to enzymatic reduction [54]. However, upon treatment with

cytoplasmic MsrB7 for 1 h in the presence of 10 mM DTT, transferase activity is restored up to 70 and 100% for GSTF2 and GSTF3, respectively [29]. In this study, the authors focus only on the methionine oxidation rather than both methionine and Cys oxidation, as both GSTF2 and GSTF3 do not contain Cys residues, unlike GSTU23, which contains three Cys residues (Fig. S3).

The inability of Msr enzymes to recover the activity of GSTU23 following 200 µM H_2O_2 oxidation led to the exploration of alternative oxidative modifications. Mass spectrometry of oxidized $GSTU23_{ox200}$ demonstrated disulfide formation between Cys65-Cys110 and Cys65-Cys189 (Table 1), which could be attributed to either inter- or intramolecular disulfide bond formation. However, on a non-reducing gel, the oxidized form of GSTU23 is observed to be monomeric (Fig. S1), thereby indicating that inter-molecular disulfides, if present, constitute only a minor population or are mass spectrometric induced artifacts. Based on the crystal structure of GSTU23, the most likely intramolecular disulfide to occur would be between Cys65 and Cys110 (Fig. S3-B), whereby a folding motion across the active site cleft would be required to bring the respective sulfurs within the required interatomic contact distances. Such a motion around the active site of GST has been *in silico* modeled by normal mode analysis for the structurally homologous *A. thaliana* DHAR2 and human chloride intracellular channel protein 1 (CLIC1) [55, 56]. The third GSTU23 Cys residue, Cys189, on the other hand, is located on the reverse face of the enzyme, distant from Cys65 and Cys110 and unlikely to participate in intra-molecular disulfide formation without extensive structural rearrangements (Fig. S3-B). Therefore, Cys65-Cys189 together with Cys110-Cys110 are most likely both minor populations of inter-molecular disulfides induced during sample preparation and/or mass spectrometry analysis.

To understand the influence of oxidation on the cysteine residues of GSTU23, the transferase activities of the GSTU23 C65S and C110S mutants were compared with that of the WT in the presence of 100 µM and 200 µM H_2O_2 (Fig. 4). We showed the important role of Cys65 in making a disulfide bond with Cys110. In addition, the transferase activity of GSTU23 C110S decreases after incubation with 200 µM H_2O_2, which highlights the sensitivity of Cys65 to oxidation (Fig. 4C). Also in the crystal structure, Cys65 was found to be over-oxidized to a sulfinic acid (Fig. 8C). This shows the importance of the Cys65-Cys110 disulfide in preventing Cys and Met over-oxidation near the active site under hydrogen peroxide stress.

An inhibitory intramolecular disulfide between Cys65 and Cys110 could possibly be a target for a thioredoxin (Trx) or a glutaredoxin (Grx), thereby providing an additional enzymatic redox regulation of GSTU23, functioning next to the methionine sulfoxide reductases [57]. Grx can reduce its substrates either through a mono-thiol mechanism, where

a glutathionylated protein is a substrate of Grx, or a di-thiol mechanism, where an exchange in disulfide bond between reduced Grx and oxidized substrate occurs [57, 58]. In this study, we show the recycling of $GSTU23_{ox200}$ by reduced Grx, which uses a dithiol mechanism (Fig. 2), where the N-terminal Cys thiol performs a nucleophilic attack on the $GSTU23_{ox200}$ disulfide, which results in the formation of a mixed disulfide. Subsequently, the C-terminal Cys of Grx reduces this disulfide, resulting in the release of reduced GSTU23 and oxidized Grx. A GSH molecule then performs a nucleophilic attack on the mixed disulfide, which results in the glutathionylation of Grx. Another molecule of GSH performs a nucleophilic attack, which releases reduced Grx and oxidized glutathione (GSSG). The GSSG is then recycled by glutathione reductase (GR), an NADPH-dependent flavoenzyme (Fig. 12) [59].

In this study, the influence of 100 µM and 200 µM H_2O_2 on the transferase activity of GSTU23 is studied. However, aside from the transferase activity, some GST family members also possess glutathione peroxidase activity [10, 11, 60], which contributes to plant survival under biotic and abiotic stress conditions [60]. Important to note is that glutathione transferases act as weak peroxidases with rate constants, which are usually significantly lower than glutathione peroxidases and peroxiredoxins [61]. To determine whether GSTU23 has peroxidase activity and whether oxidation with 100 µM or 200 µM H_2O_2 causes an increase or a decrease in its peroxidase activity, the FOX assay was used. The results of this experiment show that indeed GSTU23 possesses glutathione peroxidase activity and upon oxidation with 100 µM, where methionine sulfoxide is the major post-translational modification (PTM) or 200 µM H_2O_2, where disulfide bond formation is the major PTM, its peroxidase activity decreases, indicating its sensitivity to oxidation (Fig. S4).

To further understand the role of GSTU23 Cys residues under oxidative stress and how they influence the function of GSTU23, we performed a steady-state kinetic and thermodynamic study. The results of both studies on $GSTU23_{red}$ and $GSTU23_{ox200}$ indicate that the formation of a disulfide bond causes a less flexible environment close to the binding site as Cys110 is located near the H-site and Cys65, near the G-site. A disulfide bond formed between these two Cys residues could disturb the binding of the two substrates, GSH and CDNB. When comparing the k_{cat}/K_m constants for the transferase activity of $GSTU23_{red}$ (6.79×10^3 $M^{-1}s^{-1}$) and $GSTU23_{ox200}$ (8.75×10^3 $M^{-1}s^{-1}$), it is observed that under oxidative stress, $GSTU23_{ox200}$ has a slightly higher catalytic specificity constant. Although we observed a lower k_{cat} under oxidative stress, the kinetic efficiency is maintained by adapting the active site in such a way that it lowers the K_m.

To understand the slight increase in catalytic efficiency of $GSTU23_{ox200}$, the transition state thermodynamic parameters were determined. We observed that the $E:S_{red}$ complex requires less energy to reach the transition state conformation compared to $E:S_{ox200}$, while $E:S_{ox200}$

complex activation is more favourable than $E:S_{red}$. The conversion of K_m values in ΔG°' showed a higher release of energy for $E:S_{ox200}$ (-5.5 ± 0.7 kcal.mol^{-1}) formation in contrast with the $E:S_{red}$ form (-4.4 ± 0.3 kcal.mol^{-1}). These results suggest that $GSTU23_{ox200}$ forms a more favourable E:S complex to overcome the decrease in k_{cat} induced by disulfide bond formation and/or sulfoxidation in a similar mechanism observed for mesophilic and psychrophilic (cold adapted) enzymes (Fig. 5) [62]. Cold adapter enzymes evolved a mechanism to maintain their catalytic efficiencies where $\Delta H^{\#}$ is lowered due to the lower availability of heat in the environment however, a $\Delta S^{\#}$ decrease counterbalances the gain in activity, leading to a similar $\Delta G^{\#}$ as its mesophilic homologue [62].

In our study, we could visualize modifications on both Met and Cys residues on the crystal structure of oxidized GSTU23, as they are most sensitive to oxidation. Focusing first on methionine oxidation, we observed $MetSO_2$ formation on Met14, which is located close to the H-site and near the catalytic Ser13, and sulfoxidation of Met47, which is distant from the G- and H- sites (Fig. 7 and 8, Fig. S3). Although Met47 was crystallographically determined to form an *S*-sulfoxide, the preferred sulfoxidation stereoisomer for Met14 could not be reliably postulated due to its overoxidation. If Met14 preferentially forms a *R*-sulfoxide stereoisomer, this would explain the transferase activity results, where both MsrA and MsrB are needed to restore the activity and regulate GSTU23 activity of GSTU23 oxidized in 100 µM H_2O_2. Important to note is that $GSTU23_{ox100}$ transferase activity was not 100% recovered, which could be due to a minor population within the sample carrying methionine sulfone as is observed in the GSTU23 oxidized crystal structure (Fig. 8A). Despite Met14 being stacked between Trp114 and Tyr107, which would make it less prone to oxidation [63], we could show that this residue is sensitive to oxidation and any modification on it would disrupt GSH binding or activation by the catalytic Ser13.

Aside from Met oxidation, within the crystal structure of oxidized GSTU23, Cys oxidation was also observed on Cys65 and Cys110, but not on Cys189. An interesting feature observed within the oxidized crystal structure is shown in figure 8, where enrolment of the α-4 helix makes Cys110 to move within ~3 Å from Met14SO, and get partially oxidized to a sulfenic acid. One hypothesis might be a transfer of oxygen from the Met14SO to the Cys110, which could form a sulfenic acid on Cys110, which is followed by Cys110-Cys65 disulfide formation. Although this is a rather speculative interpretation, similar sulfur oxygen transfer is observed in Msr-enzymes [15, 64], where the nucleophilic Cys attacks a MetSO substrate, releasing methionine and a sulfenic acid is formed on Cys. Next, a disulfide is formed with one of the two resolving Cys residues.

A structural change upon oxidation was confirmed with CD measurements. When we oxidized GSTU23 with different concentrations of hydrogen peroxide, secondary structure analysis shows a decrease in ß-sheet content. A decrease in the molar ellipticity at 208 nm

also suggests an increase in α-helical content. For the case of $GSTU23_{ox100}$, this could be due to the local unfolding around Cys110, as is observed in our oxidized X-ray crystal structure of GSTU23 (Fig. 9). And for the case of $GSTU23_{ox200}$ and $GSTU23_{ox500}$, the changes could be due to the disulfide bond (Cys65- Cys110) formed between the Cys residues leading to an overall secondary structural change. Though the Cys residues are located far away from each other, the formation of a disulfide bond could still be possible upon oxidation, as is the case of human CLIC1, an intracellular chloride ion channel, which is structurally very similar to GSTU23 but with a completely different function. Within the reduced structure (PDB ID: 1K0M), the Cys residues (Cys24 and Cys59) are distant from each other; while within the oxidized crystal structure (PDB ID: 1RK4), they form a disulfide bond, causing a decrease in the ß-sheet content (Fig. S5). CLIC1 requires this disulfide bond formation to expose a hydrophobic surface, which helps CLIC1 to be inserted into the membrane [56, 65].

5. Conclusions

GSTU23 is able to cope with oxidative stress. At mild oxidative stress conditions sulfoxides are formed on methionines, which can be reduced by methionine sulfoxide reductases. Under higher oxidative stress conditions, a disulfide bond is formed, which can be recycled by glutaredoxin (Fig. 12). In both cases GSTU23 stays operational with almost the same catalytic specificity. By making a structural environment that favours enzyme substrate complex formation, GSTU23 is able to rescue the drop in k_{cat} and to maintain its functionality under oxidative stress.

Conflict of interest: The authors declare that they have no conflicts of interest with the contents of this article.

Funding information

This work was made possible thanks to financial support from (i) Vlaams Instituut voor Biotechnologie (VIB), (ii) FWO PhD fellowship granted to MAT (iii) Fonds voor Wetenschappelijk Onderzoek Vlaanderen (FWO project G0D7914N: “Sulfenomics: oxidatieve schakelaars in planten. Hoe zwavelhoudende planteneiwitten via 'agressieve' zuurstof praten”), (iv) Omics@VIB Marie Curie COFUND fellowship to IVM, (v) the equipment grant HERC16 from the Hercules foundation and (vi) the Strategic Research Programme (SRP34) of the VUB granted to JM.

Author contributions

MAT, LR and JM contributed to the design of the experiments. Biochemical assays, kinetics, thermodynamics and CD experiments were performed by MAT and analyzed by MAT, LR and JM. Crystallization was performed by KW and IVM, and X-ray crystal structures were solved by IVM and DY. MS was performed by DV. MAT, DY, LR, IVM, KG, FB and JM wrote the manuscript.

Acknowledgements

We thank the beamline scientist at the Diamond Light Source beamline IO4 and I24 for their

technical support. We thank Jean-Pierre Jacquot of University of Lorraine, Nancy for giving us *Pt*-GrxC1.

REFERENCES

[1] B.P. DeRidder, D.P. Dixon, D.J. Beussman, R. Edwards, P.B. Goldsbrough, Induction of glutathione S-transferases in Arabidopsis by herbicide safeners, Plant Physiol, 130 (2002) 1497-1505.

[2] D.P. Dixon, T. Hawkins, P.J. Hussey, R. Edwards, Enzyme activities and subcellular localization of members of the Arabidopsis glutathione transferase superfamily, J Exp Bot, 60 (2009) 1207-1218.

[3] K.A. Marrs, V. Walbot, Expression and RNA splicing of the maize glutathione S-transferase Bronze2 gene is regulated by cadmium and other stresses, Plant Physiol, 113 (1997) 93-102.

[4] L. Prade, R. Huber, B. Bieseler, Structures of herbicides in complex with their detoxifying enzyme glutathione S-transferase - explanations for the selectivity of the enzyme in plants, Structure, 6 (1998) 1445-1452.

[5] R. Thom, I. Cummins, D.P. Dixon, R. Edwards, D.J. Cole, A.J. Lapthorn, Structure of a tau class glutathione S-transferase from wheat active in herbicide detoxification, Biochemistry, 41 (2002) 7008-7020.

[6] B. McGonigle, S.J. Keeler, S.M. Lau, M.K. Koeppe, D.P. O'Keefe, A genomics approach to the comprehensive analysis of the glutathione S-transferase gene family in soybean and maize, Plant Physiol, 124 (2000) 1105-1120.

[7] R. Thom, D.P. Dixon, R. Edwards, D.J. Cole, A.J. Lapthorn, The structure of a zeta class glutathione S-transferase from *Arabidopsis thaliana*: characterisation of a GST with novel active-site architecture and a putative role in tyrosine catabolism, J Mol Biol, 308 (2001) 949-962.

[8] D.P. Dixon, R. Edwards, Glutathione transferases, Arabidopsis Book, 8 (2010) e0131.

[9] M. Deponte, Glutathione catalysis and the reaction mechanisms of glutathione-dependent enzymes, Biochim Biophys Acta, 1830 (2013) 3217-3266.

[10] U. Wagner, R. Edwards, D.P. Dixon, F. Mauch, Probing the diversity of the Arabidopsis glutathione S-transferase gene family, Plant Mol Biol, 49 (2002) 515-532.

[11] E. Nutricati, A. Miceli, F. Blando, L. De Bellis, Characterization of two *Arabidopsis thaliana* glutathione S-transferases, Plant Cell Rep, 25 (2006) 997-1005.

[12] I. Cummins, D.J. Cole, R. Edwards, A role for glutathione transferases functioning as glutathione peroxidases in resistance to multiple herbicides in black-grass, Plant J, 18 (1999) 285-292.

[13] V.P. Roxas, R.K. Smith, Jr., E.R. Allen, R.D. Allen, Overexpression of glutathione S-transferase/glutathione peroxidase enhances the growth of transgenic tobacco seedlings during stress, Nat Biotechnol, 15 (1997) 988-991.

[14] G. Roos, J. Messens, Protein sulfenic acid formation: from cellular damage to redox regulation, Free Radic Biol Med, 51 (2011) 314-326.

[15] A. Drazic, J. Winter, The physiological role of reversible methionine oxidation, Biochim Biophys Acta, 1844 (2014) 1367-1382.

[16] J.M. Denu, K.G. Tanner, Specific and reversible inactivation of protein tyrosine phosphatases by hydrogen peroxide: evidence for a sulfenic acid intermediate and implications for redox regulation, Biochemistry, 37 (1998) 5633-5642.

[17] E.R. Stadtman, Protein oxidation and aging, Free Radic Res, 40 (2006) 1250-1258.

[18] C. Jacob, G.I. Giles, N.M. Giles, H. Sies, Sulfur and selenium: the role of oxidation state in protein structure and function, Angew Chem Int Ed Engl, 42 (2003) 4742-4758.

[19] F. Aslund, K.D. Berndt, A. Holmgren, Redox potentials of glutaredoxins and other thiol-disulfide oxidoreductases of the thioredoxin superfamily determined by direct protein-protein redox equilibria, J Biol Chem, 272 (1997) 30780-30786.

[20] E.S. Arner, A. Holmgren, Physiological functions of thioredoxin and thioredoxin reductase, Eur J Biochem, 267 (2000) 6102-6109.

[21] D. Ritz, J. Beckwith, Roles of thiol-redox pathways in bacteria, Annu Rev Microbiol, 55 (2001) 21-48.

[22] A. Drazic, H. Miura, J. Peschek, Y. Le, N.C. Bach, T. Kriehuber, J. Winter, Methionine oxidation activates a transcription factor in response to oxidative stress, Proc Natl Acad Sci U S A, 110 (2013) 9493-9498.

[23] M.J. Emes, Oxidation of methionine residues: the missing link between stress and signalling responses in plants, Biochem J, 422 (2009) e1-2.

[24] V.S. Sharov, D.A. Ferrington, T.C. Squier, C. Schoneich, Diastereoselective reduction of protein-bound methionine sulfoxide by methionine sulfoxide reductase, FEBS Lett, 455 (1999) 247-250.

[25] R. Grimaud, B. Ezraty, J.K. Mitchell, D. Lafitte, C. Briand, P.J. Derrick, F. Barras, Repair of oxidized proteins. Identification of a new methionine sulfoxide reductase, J Biol Chem, 276 (2001) 48915-48920.

[26] M.J. Davies, The oxidative environment and protein damage, Biochim Biophys Acta, 1703 (2005) 93-109.

[27] A. Sadanandom, Z. Poghosyan, D.J. Fairbairn, D.J. Murphy, Differential regulation of plastidial and cytosolic isoforms of peptide methionine sulfoxide reductase in Arabidopsis, Plant Physiol, 123 (2000) 255-264.

[28] C. Vieira Dos Santos, S. Cuine, N. Rouhier, P. Rey, The Arabidopsis plastidic methionine sulfoxide reductase B proteins. Sequence and activity characteristics, comparison of the expression with plastidic methionine sulfoxide reductase A, and induction by photooxidative stress, Plant Physiol, 138 (2005) 909-922.

[29] S.H. Lee, C.W. Li, K.W. Koh, H.Y. Chuang, Y.R. Chen, C.S. Lin, M.T. Chan, MSRB7 reverses oxidation of GSTF2/3 to confer tolerance of *Arabidopsis thaliana* to oxidative stress, J Exp Bot, 65 (2014) 5049-5062.

[30] S. Jacques, B. Ghesquiere, P.J. De Bock, H. Demol, K. Wahni, P. Willems, J. Messens, F. Van Breusegem, K. Gevaert, Protein Methionine Sulfoxide Dynamics in *Arabidopsis thaliana* under Oxidative Stress, Mol Cell Proteomics, 14 (2015) 1217-1229.

[31] M.A. Tossounian, B. Pedre, K. Wahni, H. Erdogan, D. Vertommen, I. Van Molle, J. Messens, *Corynebacterium diphtheriae* methionine sulfoxide reductase a exploits a unique mycothiol redox relay mechanism, J Biol Chem, 290 (2015) 11365-11375.

[32] W.H. Habig, M.J. Pabst, W.B. Jakoby, Glutathione S-transferases. The first enzymatic step in mercapturic acid formation, J Biol Chem, 249 (1974) 7130-7139.

[33] W. Kabsch, Xds, Acta Crystallogr D Biol Crystallogr, 66 (2010) 125-132.

[34] P. Emsley, K. Cowtan, Coot: model-building tools for molecular graphics, Acta Crystallogr D Biol Crystallogr, 60 (2004) 2126-2132.

[35] P.V. Afonine, R.W. Grosse-Kunstleve, N. Echols, J.J. Headd, N.W. Moriarty, M. Mustyakimov, T.C. Terwilliger, A. Urzhumtsev, P.H. Zwart, P.D. Adams, Towards automated crystallographic structure refinement with phenix.refine, Acta Crystallogr D Biol Crystallogr, 68 (2012) 352-367.

[36] Schrodinger, LLC, The PyMOL Molecular Graphics System, Version 1.8, in, 2015.

[37] S. Pyr Dit Ruys, X. Wang, E.M. Smith, G. Herinckx, N. Hussain, M.H. Rider, D. Vertommen, C.G. Proud, Identification of autophosphorylation sites in eukaryotic elongation factor-2 kinase, Biochem J, 442 (2012) 681-692.

[38] S. Choi, J. Jeong, S. Na, H.S. Lee, H.-Y. Kim, K.-J. Lee, E. Paek, New algorithm for the identification of intact disulfide linkages based on fragmentation characteristics in tandem mass spectra, J Proteome Res, 9 (2010) 626-635.

[39] K. Van Laer, L. Buts, N. Foloppe, D. Vertommen, K. Van Belle, K. Wahni, G. Roos, L. Nilsson, L.M. Mateos, M. Rawat, N.A. van Nuland, J. Messens, Mycoredoxin-1 is one of the missing links in the oxidative stress defence mechanism of Mycobacteria, Mol Microbiol, 86 (2012) 787-804.

[40] A.F. Villadangos, K. Van Belle, K. Wahni, V.T. Dufe, S. Freitas, H. Nur, S. De Galan, J.A. Gil, J.F. Collet, L.M. Mateos, J. Messens, Corynebacterium glutamicum survives arsenic stress with arsenate reductases coupled to two distinct redox mechanisms, Mol Microbiol, 82 (2011) 998-1014.

[41] J. Jaeger, K. Sorensen, S.P. Wolff, Peroxide accumulation in detergents, J Biochem Biophys Methods, 29 (1994) 77-81.

[42] K.M. Ivanetich, R.D. Goold, A rapid equilibrium random sequential bi-bi mechanism for human placental glutathione S-transferase, Biochim Biophys Acta, 998 (1989) 7-13.

[43] I. Jakobson, P. Askelof, M. Warholm, B. Mannervik, A steady-state-kinetic random mechanism for glutathione S-transferase A from rat liver. A model involving kinetically significant enzyme-product complexes in the forward reaction, Eur J Biochem, 77 (1977) 253-262.

[44] B. Nay, D. Fournier, A. Baudras, B. Baudras, Mechanism of an insect glutathione S-transferase: kinetic analysis supporting a rapid equilibrium random sequential mechanism with housefly I1 isoform, Insect Biochem Mol Biol, 29 (1999) 71-79.

[45] G. Ricci, P. Turella, F. De Maria, G. Antonini, L. Nardocci, P.G. Board, M.W. Parker, M.G. Carbonelli, G. Federici, A.M. Caccuri, Binding and kinetic mechanisms of the zeta class glutathione transferase, J Biol Chem, 279 (2004) 33336-33342.

[46] V.L. Schramm, R. Mccluskey, F.A. Emig, G. Litwack, Kinetic-studies and active site-binding properties of glutathione S-transferase using spin-labeled glutathione, a product analog, J Biol Chem, 259 (1984) 714-722.

[47] I.H. Segel, Enzyme-kinetics: behavior and analysis of rapid equilibrium and steady-state enzyme-systems, Cc/Life Sci, (1987) 14-14.

[48] C.R. Simmons, K. Krishnamoorthy, S.L. Granett, D.J. Schuller, J.E. Dominy, Jr., T.P. Begley, M.H. Stipanuk, P.A. Karplus, A putative Fe2+-bound persulfenate intermediate in cysteine dioxygenase, Biochemistry, 47 (2008) 11390-11392.

[49] C.M. Driggers, R.B. Cooley, B. Sankaran, L.L. Hirschberger, M.H. Stipanuk, P.A. Karplus, Cysteine dioxygenase structures from pH 4 to 9: Consistent Cys-persulfenate formation at intermediate pH and a Cys-bound enzyme at higher pH, J Mol Biol, 425 (2013) 3121-3136.

[50] G. Xu, M.R. Chance, Radiolytic modification of sulfur-containing amino acid residues in model peptides: fundamental studies for protein footprinting, Anal Chem, 77 (2005) 2437-2449.

[51] K.G. Kilili, N. Atanassova, A. Vardanyan, N. Clatot, K. Al-Sabarna, P.N. Kanellopoulos, A.M. Makris, S.C. Kampranis, Differential roles of tau class glutathione S-transferases in oxidative stress, J Biol Chem, 279 (2004) 24540-24551.

[52] P. Kerchev, B. De Smet, C. Waszczak, J. Messens, F. Van Breusegem, Redox Strategies for Crop Improvement, Antioxid Redox Signal, 23 (2015) 1186-1205.

[53] C.C. Winterbourn, M.B. Hampton, Thiol chemistry and specificity in redox signaling, Free Radic Biol Med, 45 (2008) 549-561.

[54] P. Reinemer, L. Prade, P. Hof, T. Neuefeind, R. Huber, R. Zettl, K. Palme, J. Schell, I. Koelln, H.D. Bartunik, B. Bieseler, Three-dimensional structure of glutathione S-transferase from Arabidopsis thaliana at 2.2 A resolution: structural characterization of herbicide-conjugating plant glutathione S-transferases and a novel active site architecture, J Mol Biol, 255 (1996) 289-309.

[55] N. Bodra, D. Young, L. Astolfi Rosado, A. Pallo, K. Wahni, F. De Proft, J. Huang, F. Van Breusegem, J. Messens, Arabidopsis thaliana dehydroascorbate reductase 2: Conformational flexibility during catalysis, Sci Rep, 7 (2017) 42494.

[56] D.R. Littler, S.J. Harrop, W.D. Fairlie, L.J. Brown, G.J. Pankhurst, S. Pankhurst, M.Z. DeMaere, T.J. Campbell, A.R. Bauskin, R. Tonini, M. Mazzanti, S.N. Breit, P.M. Curmi, The intracellular chloride ion channel protein CLIC1 undergoes a redox-controlled structural transition, J Biol Chem, 279 (2004) 9298-9305.

[57] C. Berndt, C.H. Lillig, A. Holmgren, Thiol-based mechanisms of the thioredoxin and glutaredoxin systems: implications for diseases in the cardiovascular system, Am J Physiol Heart Circ Physiol, 292 (2007) H1227-1236.

[58] J.H. Bushweller, F. Aslund, K. Wuthrich, A. Holmgren, Structural and functional characterization of the mutant Escherichia coli glutaredoxin (C14----S) and its mixed disulfide with glutathione, Biochemistry, 31 (1992) 9288-9293.

[59] P. Nagy, Kinetics and mechanisms of thiol-disulfide exchange covering direct substitution and thiol oxidation-mediated pathways, Antioxid Redox Signal, 18 (2013) 1623-1641.

[60] E. Horvath, K. Bela, C. Papdi, A. Galle, L. Szabados, I. Tari, J. Csiszar, The role of Arabidopsis glutathione transferase F9 gene under oxidative stress in seedlings, Acta Biol Hung, 66 (2015) 406-418.

[61] S. Toppo, L. Flohe, F. Ursini, S. Vanin, M. Maiorino, Catalytic mechanisms and specificities of glutathione peroxidases: variations of a basic scheme, Biochim Biophys Acta, 1790 (2009) 1486-1500.

[62] G. Feller, C. Gerday, Psychrophilic enzymes: molecular basis of cold adaptation, Cell Mol Life Sci, 53 (1997) 830-841.

[63] J.C. Aledo, F.R. Canton, F.J. Veredas, Sulphur atoms from methionines interacting with aromatic residues are less prone to oxidation, Sci Rep, 5 (2015) 16955.

[64] S. Boschi-Muller, S. Azza, S. Sanglier-Cianferani, F. Talfournier, A. Van Dorsselear, G. Branlant, A sulfenic acid enzyme intermediate is involved in the catalytic mechanism of peptide methionine sulfoxide reductase from Escherichia coli, J Biol Chem, 275 (2000) 35908-35913.

[65] S.J. Harrop, M.Z. DeMaere, W.D. Fairlie, T. Reztsova, S.M. Valenzuela, M. Mazzanti, R. Tonini, M.R. Qiu, L. Jankova, K. Warton, A.R. Bauskin, W.M. Wu, S. Pankhurst, T.J. Campbell, S.N. Breit, P.M. Curmi, Crystal structure of a soluble form of the intracellular chloride ion channel CLIC1 (NCC27) at 1.4-A resolution, J Biol Chem, 276 (2001) 44993-45000.

[66] D. Liebschner, P.V. Afonine, N.W. Moriarty, B.K. Poon, O.V. Sobolev, T.C. Terwilliger, P.D. Adams, Polder maps: improving OMIT maps by excluding bulk solvent, Acta Crystallogr D Struct Biol, 73 (2017) 148-157.

FIGURE LEGENDS

Fig. 1. Msr enzymes and DTT restore the transferase activity of oxidized GSTU23. Bar graphs show the rate constants, *k* (s^{-1}), of $GSTU23_{red}$ and $GSTU23_{ox100}$ under different conditions. (*A*) Upon oxidation of $GSTU23_{red}$ with 100 µM H_2O_2, $GSTU23_{ox100}$ is formed, which significantly ($p \leq 0.005$, depicted as *) loses 33% of its activity, which is almost fully recovered upon incubation with 40 µM MsrA and MsrB for 30 min at 25ºC. When treated with DTT, $GSTU23_{ox100}$ activity is marginally recovered. As a control, $GSTU23_{red}$ was incubated with MsrA or MsrB. (*B*) Upon oxidation of $GSTU23_{red}$ with 200 µM H_2O_2, $GSTU23_{ox200}$ is formed, and its activity drops significantly ($p \leq 0.005$, depicted as *) to 41%. Upon incubation with MsrA or MsrB, the activity is only marginally regained to 54 and 53% respectively. Incubation of $GSTU23_{ox200}$ with 2 mM DTT restores the activity to 93%. Data from 3 independent technical experiments are presented as a mean ± SD and the graph was generated using GraphPad Prism7.

Fig. 2. Oxidized GSTU23 is recycled by the Grx/GR/NADPH pathway. (*A*) Bar graph compares the rate constants *k* (s^{-1}) of $GSTU23_{ox200}$ incubated with 10-fold excess of reduced Trx or GrxC1. The results show an increase in the initial transferase activity of GSTU23ox200 from 41% to 97% upon incubation with Grx, while incubation with Trx only marginally recovers the transferase activity. (*B*) Bar graphs compare the rate constants *k* (s^{-1}) of $GSTU23_{ox200}$ when coupled to the Trx/TrxR/NADPH or the Grx/GR/NADPH pathway. The results show that GSTU23ox200 is recycled by the Grx/GR/NADPH pathway, while no NADPH consumption is observed when coupled to the Trx/TrxR/NADPH pathway. Data from 2 independent technical experiments are presented as a mean ± SD and the graph was generated using GraphPad Prism7.

Fig. 3. Methionine and cysteine oxidation on oxidized GSTU23. (*A*) Identification of Met-sulfoxide on Met47 of $GSTU23_{ox100}$. The MS/MS spectrum shows data obtained from a triply charged parent ion with a m/z-value of 562.6 Th. The y- and b-series of ions allow exact localization of the methionine sulfoxide. (*B*) Mass spectrometry analysis of oxidized $GSTU23_{ox200}$ after chymotrypsin digestion revealed a triply charged parent ion of with a m/z-value of 891.1 Th, fragmentation of it allowed to identify a disulfide linkage between Cys65 and Cys110 of GSTU23 as determined by the DBond software [38]. *P**, one strand of a dipeptide; *p**, the other strand of a dipeptide; *capital letters*, fragment ions from peptide *P**; *lowercase letters*, fragment ions from peptide *p**.

Fig. 4. GSTU23 Cys to Ser mutants display a different transferase activity than WT. The bar graphs show the rate constants, *k* (s^{-1}), of GSTU23 WT (*A*), C65S (*B*) and C110S (*C*) under different oxidizing conditions (0, 100 and 200 µM H_2O_2). (*A*) Upon increase in H_2O_2 concentration, GSTU23 WT activity decreases from 100% (WT_{red}) to 67% (WT_{ox100}) and 41% (WT_{ox200}). (*B*) On the other hand, oxidation of GSTU23 C65S mutant has no influence on the transferase activity. (*C*) A different profile is observed for GSTU23 C110S mutant, where increase in H_2O_2 concentration causes a decrease in transferase activity from 100% ($C110S_{red}$) to 91% ($C110S_{ox100}$) and 67% ($C110S_{ox200}$). Data from 3 independent technical experiments are presented as a mean ± SD and the graph was generated using GraphPad Prism7.

Fig. 5. The Michaelis-Menten curves of (*A*) GSTU23$_{red}$ and (*B*) GSTU23$_{ox200}$ in the presence of a saturating concentration of GSH (5 mM) are shown. The kinetic parameter k_{cat}, K_m and the catalytic efficiency (k_{cat}/K_m) are calculated from the hyperbolic plots. Although k_{cat} and K_m are clearly different for (*A*) GSTU23$_{red}$ and (*B*) GSTU23$_{ox200}$, the difference is almost completely cancelled out in the catalytic efficiency. The data are presented as a mean ± SD of two independent technical experiments and the graph was generated using GraphPad Prism7.

Fig. 6. GSTU23$_{ox200}$ forms a more favourable enzyme:substrate complex. (*A*) Temperature dependence of the GSTU23 transferase activity Eyring plot of GSTU23$_{red}$ and GSTU23$_{ox200.}$ Comparison of the Eyring plot of GSTU23$_{red}$ and GSTU23$_{ox200}$, which is used to calculate the thermodynamic parameters of both states of GSTU23, which are shown in Table 2. Data from 2 independent technical experiments are presented as a mean ± SD and the graph was generated using GraphPad Prism7. (*B*) Schematic representation of a reaction coordinate comparing GSTU23$_{red}$ (dotted line) and GSTU23$_{ox200}$ (undotted line) shows that E:S$_{ox200}$ complex requires 4 kcal.mol^{-1} to reach the transition state compared to the E:S$_{red}$, while the activation of E:S$_{ox200}$ is more favourable than E:S$_{red}$. Δ1 and Δ3 stands for the energy variation of E:S to E+S and E:S# to E:S of GSTU23$_{red}$; Δ2 and Δ4 stands for the energy variation of E:S to E+S and E:S$^{\#}$ to E:S of GSTU23$_{ox200}$.

Fig. 7. GSH bound GSTU23 X-ray crystal structure. (*A*) Monomeric form of GSTU23, with an N-terminal thioredoxin (Trx)-fold domain indicated with light cyan cartoon, and a C-terminal helical bundle domain indicated with a darker cyan cartoon. The G- and H-sites are indicated by arrows, where a GSH represented in yellow sticks is bound within the G-site, and a glycerol (GOL) molecule, represented in orange sticks is bound within the H-site. The catalytic Ser13 is in stick form, which is located within the glutathione binding site. (*B*) A mesh representation around a GSH molecule bound within the G-site of GSTU23. The gray electron density around the GSH is shown at 1.2 contour level. (*C*) Ligplot representation showing the stabilization interactions GSH makes within the G-site. (*D*) Overlay of apo (cyan cartoon) and GSH bound GSTU23 (gray cartoon) G-site. In the absence of GSH, Tyr107 stabilizes the G-site through a hydrogen-bonding network in which two water molecules, Ser13, Tyr107 and Pro55 are involved. Upon GSH binding, the hydrogen-bonding network is disturbed and Tyr107 interacts with the conserved Lys53. The residues involved in the hydrogen-bonding network are in cyan stick representation, waters in red spheres, and hydrogen bonds in red dashed lines. GSH is in gray stick representation. The alpha helices and beta strands, which contain the Met and Cys residues, are indicated on the figure.

Fig. 8. Oxidative modifications of methionine and cysteine observed in the H_2O_2/NaOCl-soaked GSTU23 crystal. The oxidation of Met14 to methionine sulfone (A), Met47 to methionine *S*-sulfoxide (B), and Cys65 to sulfinic acid (C), are defined within polder omit maps contoured at 5 σ, 4 σ, and 6 σ respectively [66]. The alpha helices and beta strands, which contain the Met and Cys residues, are indicated on the figure.

Fig. 9. Conformational change of Cys110 upon oxidation. In the oxidized structure of GSTU23 (cyan), Cys110 moves to a conformation in which it is directed into the solvent-exposed cleft containing the H-site. Partial unwinding of the α-helical structure containing Cys110 and a C^{β}-C^{β}-shift

of 3 Å occurs for Cys110 relative to the reduced structure (gray). The alpha helices are indicated on the figure.

Fig. 10. Additional electron density observed at C110, located on the α4 helix, in the oxidized crystal structure of GSTU23. Positive density arising in the mF_O-DF_C omit map generated following maximum-likelihood structural refinement in phenix.refine with C110 modelled as a thiol (A), sulfenic acid (B), and persulfenate (C). The 2mF_O-DF_C density map is depicted as a gray mesh contoured at 1.5 σ, and the mF_O-DF_C omit map as a green mesh contoured at 3 σ.

Fig. 11. Change in the overall secondary structure of GSTU23 upon oxidation. (*A*) Circular dichroism far-UV spectra of GSTU23 reduced and oxidized forms. The reduced form of GSTU23 is compared with that of GSTU23 oxidized with 100 µM, 200 µM and 500 µM H_2O_2. (*B*) GSTU23 far-UV spectrum of absorbance at 208 nm, where a decrease in the relative molar ellipticity [θ] in percentage is observed upon increase of H_2O_2 concentration (0, 100, 200 and 500 µM). The curve shows a shift from ß-sheets to α-helical properties.

Fig. 12. Proposed oxidative post-translational modifications and regulatory mechanisms of GSTU23. Upon oxidation with 100 µM H_2O_2, the major post-translational modification (PTM) on $GSTU23_{ox100}$ is methionine oxidation, which is recycled by methionine sulfoxide reductase (Msr) enzymes. When the oxidant level is increased to 200 µM H_2O_2, the major modification on $GSTU23_{ox200}$ is the formation of a disulfide bond. The disulfide is recycled by reduced glutaredoxin (Grx) through a dithiol mechanism, which results in the release of reduced GSTU23 and oxidized Grx. A glutathione (GSH) molecule then reduces the disulfide formed on Grx and forms a mixed disulfide. This mixed disulfide is then reduced by another molecule of GSH, which results in the release of reduced Grx and oxidized glutathione (GSSG). The latter is recycled by glutathione reductase (GR), which uses NADPH as its final electron donor.

TABLE LEGENDS

Table 1. Summary of the mass spectrometry data on GSTU23 oxidative modifications on methionine and cysteine residues. GSTU23red was used as a control, where no oxidative modifications were observed. Based on the biochemical data, for $GSTU23_{ox100}$, methionine oxidation is observed as the major modification, and for the $GSTU23_{ox200}$, a Cys65-Cys110 disulfide, although MS shows the presence of other modifications. ND is for not detected and (-) is for no oxidative modification.

Table 2. Thermodynamic activation parameters for CDNB glutathione transferase activity with reduced and oxidized GSTU23. $\Delta(\Delta H^{\#})_{ox\text{-}red}$ and $\Delta(T\Delta S^{\#})_{ox\text{-}red}$ represent the variation of the thermodynamic parameters between $GSTU23_{ox200}$ and $GSTU23_{red}$.

Table 3. X-ray data collection and refinement statistics. Values in parentheses are for the highest resolution shell. [$]Diamond Light Source (DLS)

Figure 1

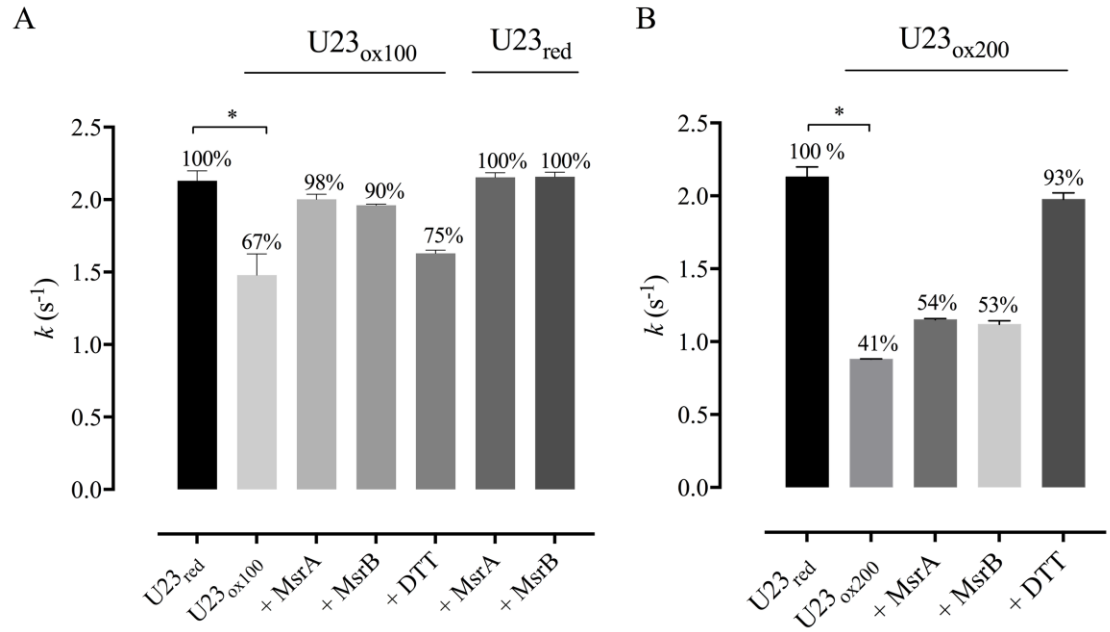

Figure 2

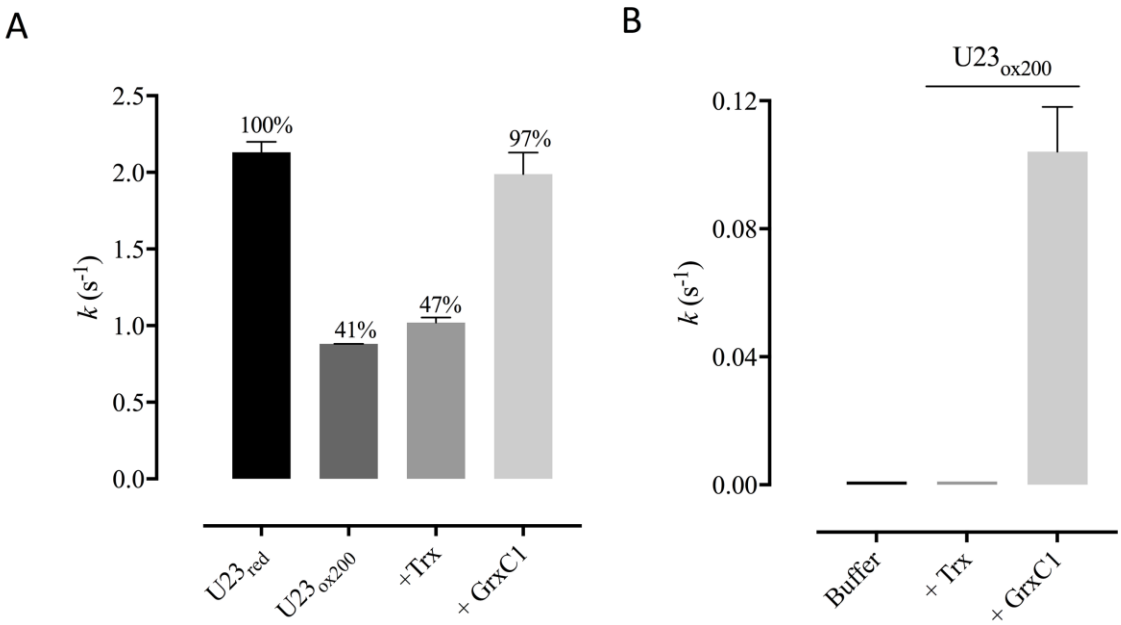

Figure 3

A

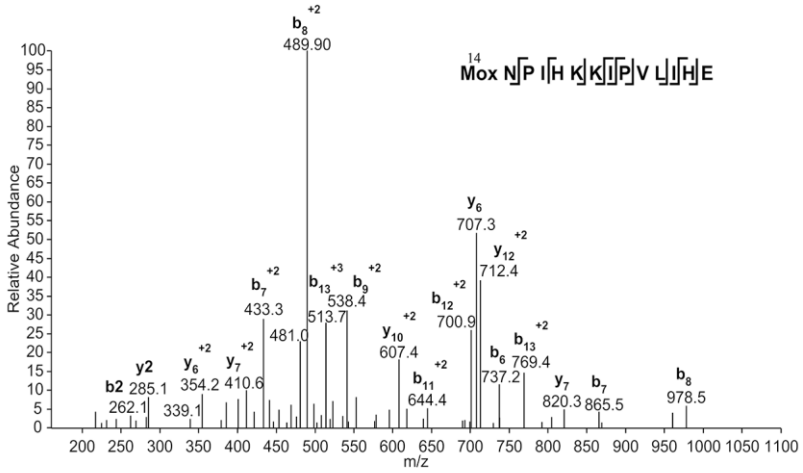

B

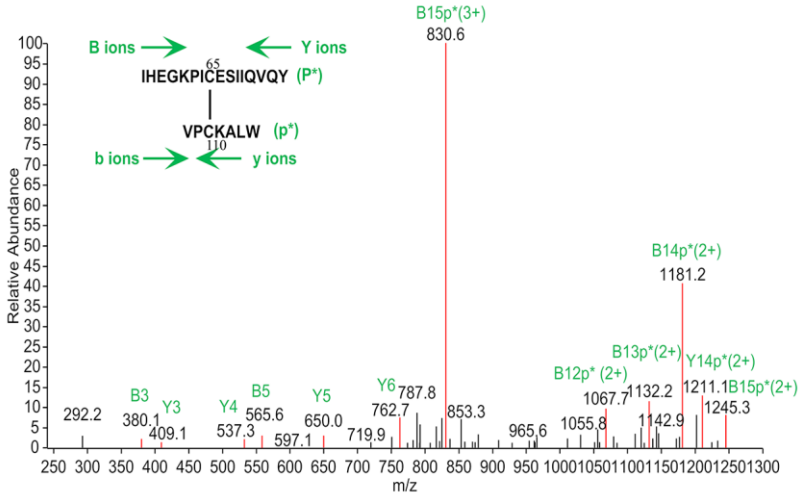

Figure 4

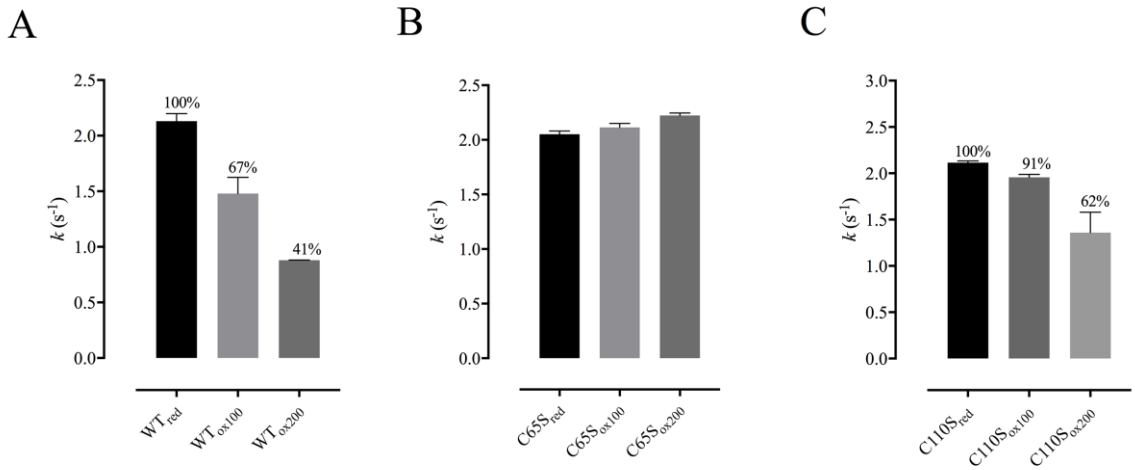

Figure 5

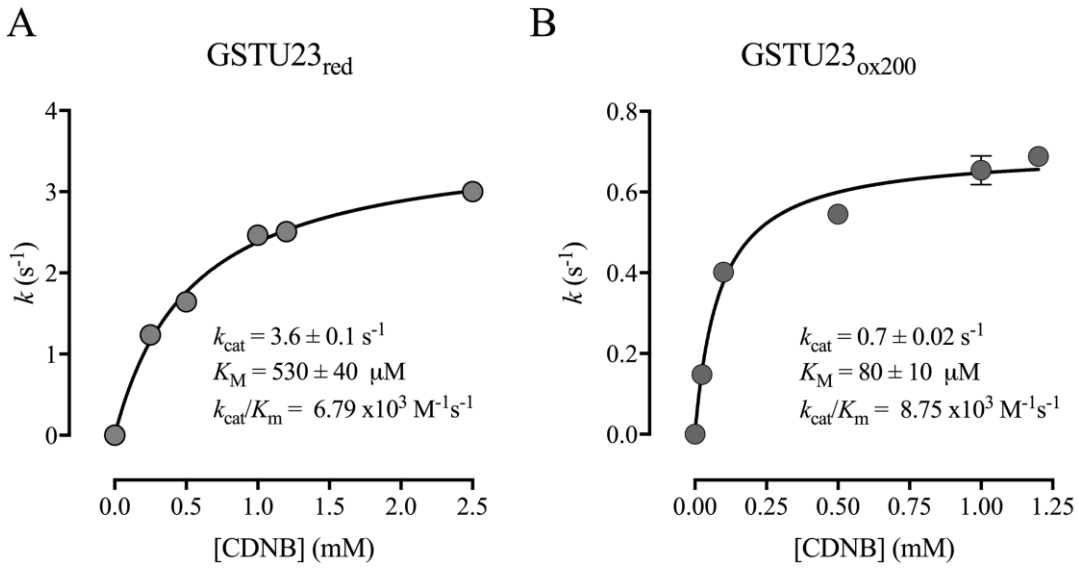

Figure 6

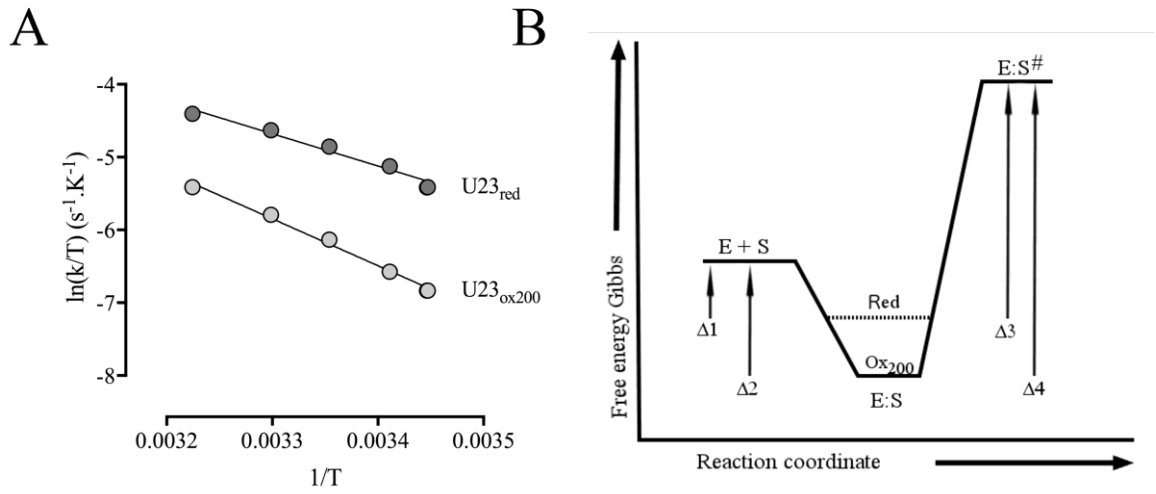

Figure 7

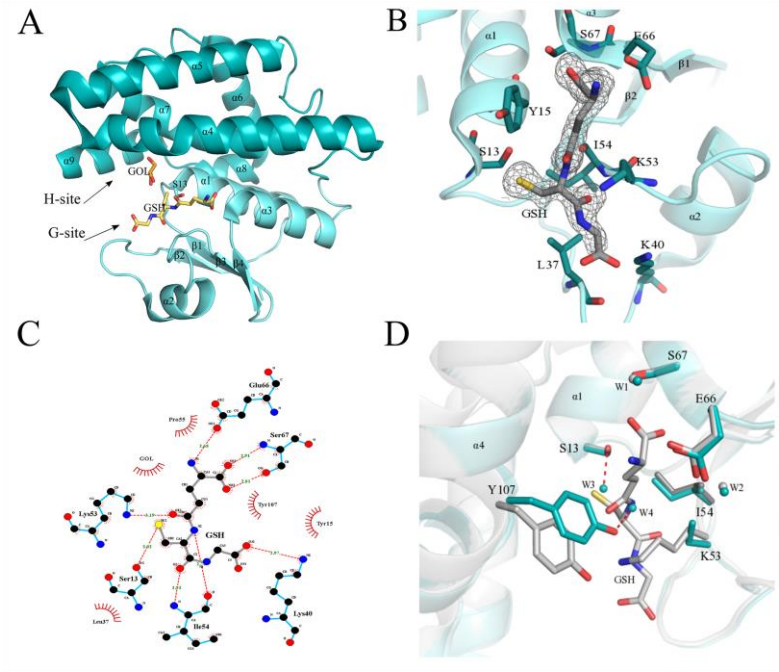

Figure 8

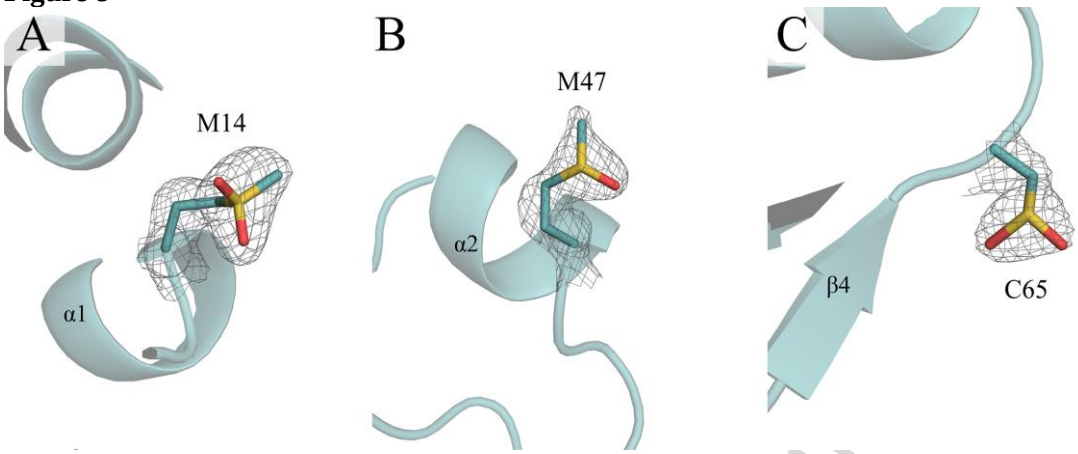

Figure 9

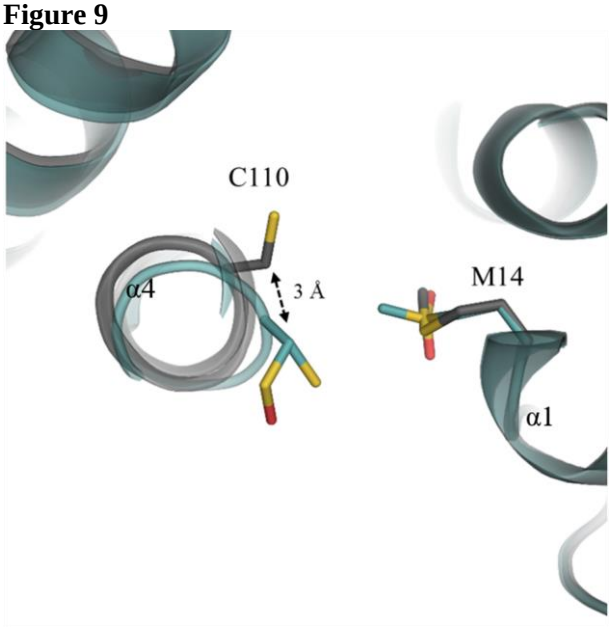

Figure 10

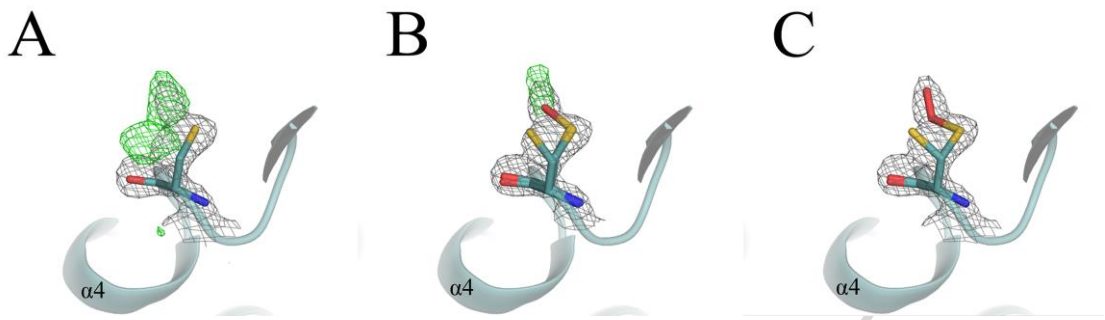

Figure 11

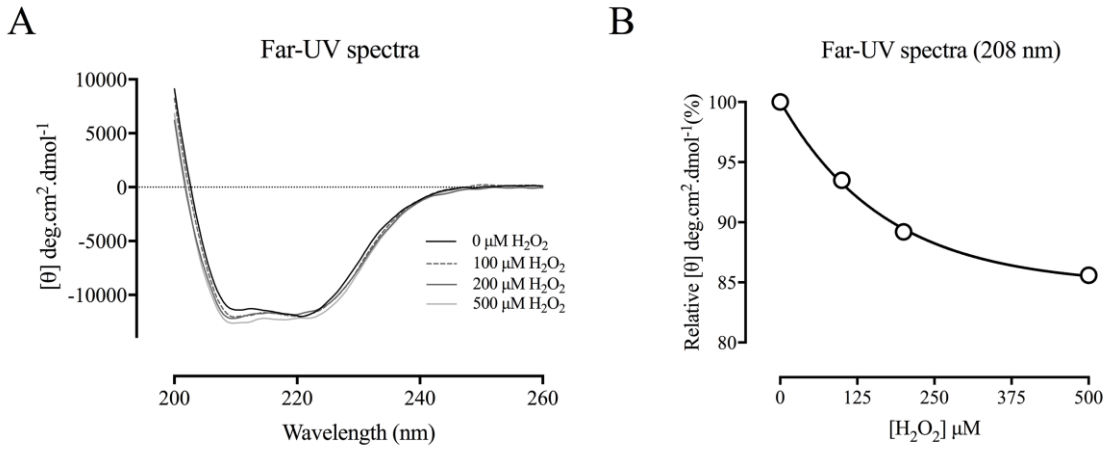

Figure 12

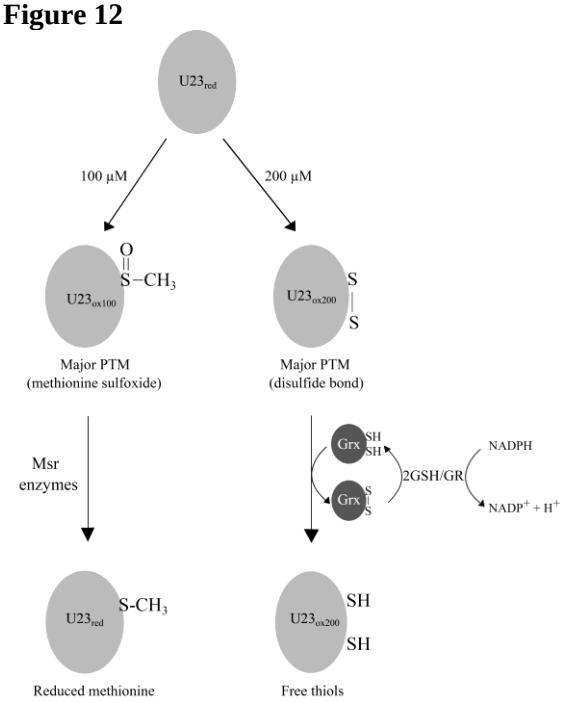

Table 1. Summary of the mass spectrometry data on GSTU23 oxidative modifications on methionine and cysteine residues. GSTU23red was used as a control, where no oxidative modifications were observed. Based on the biochemical data, for $GSTU23_{ox100}$, methionine oxidation is observed as the major modification, and for the $GSTU23_{ox200}$, a Cys65-Cys110 disulfide, although MS shows the presence of other modifications. ND is for not detected and (-) is for no oxidative modification.

oxidative modification	**methionine**	**cysteine**
$GSTU23_{red}$	-	-
$GSTU23_{ox100}$	Met47SO Met183SO	Cys65 S-S Cys110
$GSTU23_{ox200}$	ND	Cys65 S-S Cys110 Cys65 S-S Cys189 Cys110 S-S Cys110

Table 2. Thermodynamic activation parameters for CDNB glutathione S-transferase activity with reduced and oxidized GSTU23. $\Delta(\Delta H^{\#})_{ox\text{-}red}$ and $\Delta(T\Delta S^{\#})_{ox\text{-}red}$ represent the variation of the thermodynamic parameters between $GSTU23_{ox200}$ and $GSTU23_{red}$.

	E_a (kcal mol^{-1})	$\Delta H^{\#}$ (kcal mol^{-1})	$-T\Delta S^{\#}$ (kcal mol^{-1})	$* \Delta G^{\#}$ (kcal mol^{-1})	$\Delta (\Delta H^{\#})_{ox\text{-}red}$ (kcal mol^{-1})	$\Delta(-T\Delta S^{\#})_{ox\text{-}red}$ (kcal mol^{-1})
$GSTU23_{red}$	9.4 (±0.8)	8.8 (±0.8)	8.2 (±1.2)	17 (±1.7)		
$GSTU23_{ox200}$	13.4 (±0.6)	12.8 (±0.6)	4.9 (±0.3)	17.7 (±0.9)	-4.0	-3.3

$*\Delta G^{\#}$ was calculated at 25°C

Table 3. X-ray data collection and refinement statistics. Values in parentheses are for the highest resolution shell. [$]Diamond Light Source (DLS)

Dataset	**GSTU23red**	**GSTU23_GSH**	**GSTU23ox**
PDB ID	**5FQY**	**5FR4**	**5O84**
Data collection			
Beamline	I24@DLS[$]	In-house	In-house
Wavelength (Å)	0.9686	1.542	1.542
Processing			
Space group	C2	C2	C2
Cell parameters (Å/°)	88.52 50.47 113.72 90 108.62 90	87.99 50.61 113.40 90 108.57 90	85.17 50.74 57.17 90 112.47 90
Resolution, Å (outer shell)	50-1.6 (1.69-1.59)	30-1.95 (2.06-1.95)	42..64-1.88 (1.92-1.88)
Total reflections	407488 (62312)	124507 (17294)	63902 (3828)
Unique reflections	64020 (10281)	35062 (5578)	18206 (1576)
Completeness (%)	97.6 (92.9)	94.6 (85.8)	97.96 (85.73)
Multiplicity	6.4 (6.1)	3.6 (3.1)	3.5 (2.4)
CC1/2 (%)	99.7 (54.7)	99.9 (94.1)	99.7 (74)
Rmeas (%)	10.2 (139.9)	5.6 (33.3)	6.7 (66.2)
$\langle I/\sigma(I)\rangle$	16.2 (3.0)	21.5 (4.93)	16.66 (2.09)
Refinement			
Resolution range (Å)	44.18 -1.59	28.84-1.95	30.26-1.88
Percentage observed (%)	97.64	94.64	99. 5
R_{cryst} (%)	18.88	16.48	17.67
R_{free} (%)	21.98	20.90	21.44
RMS			
Bonds (Å)	0.006	0.007	0.009
Angles (°)	1.002	0.098	1.05
Ramachandran Plot			
Most favored (%)	97.12	97.11	98.51
Additionally allowed (%)	2.40	2.41	1.49
Disallowed (%)	0.48	0.48	0.0

Highlights:

- GSTU23 methionine oxidation is the major oxidative modification at lower H_2O_2 concentration
- A disulfide bond protects active site cysteines and methionines from overoxidation
- Oxidized GSTU23 is redox regulated by methionine sulfoxide reductases and glutaredoxin
- To compensate the drop in k_{cat} at a higher H_2O_2 concentration, a favorable enzyme:substrate complex is formed
- X-ray structures of oxidized GSTU23 show methionine oxidation and local unfolding around Cys110